TEL AVIV UNIVERSITY

The Iby and Aladar Fleischman Faculty of Engineering
The Zandman-Slaner School of Graduate Studies

Combination of Low-Frequency Ultrasound with Gas Bubbles as a Technological Platform for the Treatment of Tumors

Thesis submitted to the Senate of Tel-Aviv University

in partial fulfillment of the requirements for the degree of

“Doctor of Philosophy”

by

Mike Bismuth

January 2024

TEL AVIV UNIVERSITY

The Iby and Aladar Fleischman Faculty of Engineering
The Zandman-Slaner School of Graduate Studies

Combination of Low-Frequency Ultrasound with Gas Bubbles as a Technological Platform for the Treatment of Tumors

Thesis submitted to the Senate of Tel-Aviv University

in partial fulfillment of the requirements for the degree of

“Doctor of Philosophy”

by

Mike Bismuth

This research was carried out in the Department of Biomedical Engineering
Under the supervision of Dr. Tali Ilovitsh

January 2024

Acknowledgements

First, I would like to thank my supervisor, Dr. Tali Ilovitsh, for her precious mentorship and guidance. I would like to thank her for her confidence in my research capabilities, and, more significantly, for motivating me to have faith in my own abilities.

Next, I would like to thank all past and current members of the laboratory for their assistance, friendship and moral encouragement.

A warm thanks goes to my family, especially my parents, Nicole and Freddy, and my in-laws, Havatselet and Isaac, for their encouragement and support.

I am grateful to my children, Ori and Itay, for the daily joy, happiness, and smiles they bring into my life.

Lastly, I want to convey my deepest thanks to my beloved wife and best friend, Efrat, for her patience, and indispensable support.

Abstract

Focused ultrasound is a promising noninvasive therapeutic platform with attractive potential such as tumor ablation or localized drug delivery. For mechanical ablation of tumors, histotripsy is the standard procedure using high intensity focused ultrasound in a local and noninvasive way. This technique uses extremely high intensity ultrasound energy to mechanically ablate tissues, fractioning them into subcellular debris. However, conventional histotripsy raises safety concerns because of the need to focus such a high energy into the body (tens of MPa in pressure), as well as the potential for off-target effects.

To develop a theranostic platform for safe, noninvasive tumor mechanical therapy and reduce the required energy for mechanical ablation or localized drug delivery, we investigate the interaction between sound waves and ultrasound contrast agents (microbubbles and nanobubbles) to elucidate their ability to serve as efficient theranostic probes at a targeted site. Upon excitation with ultrasound, these contrast agents can oscillate, releasing high energy to the surrounding tissue. Consequently, significant mechanical bioeffects can be achieved, leading to reduced tumors cells viability and improved drug delivery. This strategy provides a unique mechanism for noninvasive and low energy ultrasound therapy.

Our first paper demonstrates that, under low-frequency excitation (250 kHz and 80 kHz), high-amplitude microbubble oscillations occur at substantially lower pressures compared to the standard megahertz ultrasonic frequencies. These enhanced microbubbles expansions are harnessed for the localized fractionation of tumors at low energies that comply with the Food and Drug Administration guidelines for imaging ultrasound applications. However, the microbubble’s large diameter of 1-4 µm confines them to intravascular applications, and therefore they were intratumorally injected, offering a minimally invasive technique.

In the second publication, we addressed this limitation by developing nanobubbles. Through comprehensive characterization of these agents and experimental observations, we provided the foundational understanding of

nanoscale bubble oscillation, leading to fundamental breakthroughs in breast cancer treatment. We demonstrated that nanobubbles, when excited in the kilohertz range, significantly enhance their oscillations, paving the way for innovative cancer therapy methods. We combined tumor-extravasating nanobubbles with low-frequency ultrasound, creating a noninvasive therapy platform for cancer surgery.

The third paper presents the use of nanobubbles for poking large holes in cancer cell membranes and facilitating drug delivery. This effect takes an advantage of the high amplitude oscillations and represents a combined strategy to enhance cancer therapy. Despite having a smaller diameter, we were able to achieve similar effects as with targeted microbubbles, suggesting that nanobubbles can serve as noninvasive drug delivery agents with similar potency.

In summary, we show that microbubbles and nanobubbles, when excited at low frequency ultrasound, can serve as low-energy cavitation nuclei for tumor histotripsy thus reducing the energy required for standard ablation procedures by more than an order of magnitude. Additionally, we harness this effect and present the use of nanobubbles for poking large holes in cancer cell membranes and facilitating drug delivery to cancer cells. Our research introduces ultrasound-based technologies for noninvasive cancer therapy using contrast agents and low-frequency ultrasound, opening new avenues for noninvasive theranostic approaches with applications in many biomedical domains.

Contents

List of abbreviations

7-AAD - 7-aminoactinomycin D

CAR - chimeric antibody-based receptor

CI - Cavitation index

DMEM - Dulbecco modified Eagle medium

EPR - Enhanced permeability and retention

FDA - Food and drug administration

FITC - Fluorescein isothiocyanate

H&E - Hematoxylin and eosin

IACUC - Institutional Animal Care and Use Committee

IHC - Immunohistochemistry

MB - Microbubble

MI - Mechanical index

NB - Nanobubble

NTC - No treatment control

PBS - Phosphate buffered saline

PBS +/+ - Phosphate buffered saline containing calcium and magnesium

PNP - Peak negative pressure

PRF - Pulse repetition frequency

HER-2 - Human epidermal growth factor receptor 2

US - Ultrasound

1. Introduction

1.1 Scientific background

The National Cancer Institute's 2023 estimation predicts almost 2 million new cancer cases in the USA, with over 600,000 patients succumbing to the disease. Breast cancer is the most common solid tumor in women responsible for 31% of female cancers [1]. Tumors frequently necessitate surgical resection as primary intervention. This preference stems from the procedure's effectiveness in reducing cancerous tissues, thereby augmenting the impact of immunotherapies and chemotherapies [2,3]. Nevertheless, the inherent risks associated with surgery, including bleeding, infections, and potential damage to surrounding structures, underscore the critical need for alternative noninvasive surgical techniques [4,5]. Various noninvasive techniques have been explored for the ablation and treatment of tumors, aiming to eliminate cancerous cells without the need for invasive surgical procedures. Among these methods are radiofrequency ablation, microwave ablation, and laser ablation, each harnessing different forms of energy to achieve tumor destruction [6,7]. These techniques have demonstrated efficacy in treating a range of cancers, offering patients alternatives to traditional surgery. However, considerable drawbacks persist. Challenges such as difficulty in uniformly treating larger tumors, limitations in precise control over ablation zones, and issues related to the depth of penetration into tissues may affect the overall effectiveness of these noninvasive approaches [7–9].

A complementary strategy for treating tumors involves enhancing the localized and targeted delivery of therapeutic agents specifically to cancer cells [10,11]. The therapeutic effectiveness of traditional chemotherapy, biological therapy and gene therapy in cancer heavily relies on the capability to transport therapeutics molecules and genes across natural barriers, such as vessel walls or tumor cell membranes. However, most agents lack specificity for tumors, resulting in elevated systemic toxicity [12,13]. Although many anticancer agents prove efficacious in eradicating monolayer tumor cells cultured in vitro, their effectiveness is notably diminished in vivo due to various barriers within the

tumor microenvironment that impede drug delivery to tumor cells [14,15]. Drug delivery strategies for tumor treatment have undergone substantial advancements to enhance the efficacy of anti-cancer agents while minimizing systemic side effects and improving tumor selectivity. A predominant strategy involves utilizing nanoparticles, such as liposomes or polymeric micelles, to encapsulate drugs and selectively target tumor tissues through passive or active targeting mechanisms [16,17]. Despite the promise of these approaches, challenges such as premature drug release, limited drug-loading capacity, and potential toxicity of delivery vehicles may impede their effectiveness [18–20]. Additionally, achieving optimal drug distribution within heterogeneous tumor environments remains a complex task [21]. Concerns about the development of resistance mechanisms and the possibility of off-target effects persist in the pursuit of effective drug delivery for tumor treatment [22,23]. Nevertheless, ongoing research endeavors aim to address these challenges and optimize drug delivery approaches for enhanced outcomes in cancer therapy.

Focused ultrasound (US) is a medical technology that harnesses the power of high-intensity US waves for therapeutic applications. This non-invasive approach enables precise targeting of tissues deep within the body without the need for surgical incisions [24,25]. In therapeutic settings, focused US has shown great promise for treating various medical conditions, including tumors [26], neurological disorders [27], and chronic pain [28]. The focused US waves generate localized heat, ablate abnormal tissues, and trigger biological responses, such as increased blood flow, drug uptake or neuromodulation [25,29–32]. With its ability to penetrate the body and precisely deliver energy to specific areas, focused US is emerging as a valuable tool in the realm of minimally invasive therapies, offering patients a potentially safer and more effective alternative to traditional treatment methods.

Focused US based ablation stands out as a promising approach with several distinct advantages. US ablation utilizes high-energy sound waves to generate heat or mechanical damage effectively targeting and destroying tissues [33,34]. One significant advantage is its real-time imaging capability, allowing for precise monitoring and adjustment during the procedure [25]. Unlike some other methods, US ablation does not involve ionizing radiation, reducing the

risk of side effects [6,25]. Additionally, US is cost effective, highly versatile and can be used for a wide range of tissues, including those in challenging locations due to its significant penetration depth [25]. Its noninvasive nature minimizes the risk of complications, promotes faster recovery, and offers a potential treatment option [26,35]. Overall, US-based ablation emerges as a safe, adaptable, and patient-friendly alternative in the landscape of noninvasive tumor treatment.

Noninvasive US ablation operates through two primary mechanisms: thermal ablation and mechanical ablation termed histotripsy [36]. Thermal ablation involves focusing the US beam to a specific region that absorbs the sound waves energy, inducing temperature increases, and causing cell death through heat. This localized temperature rise can have several effects on the tissue, including protein denaturation, cells membrane permeabilization and coagulative necrosis [37]. The overall goal of thermal ablation is to generate sufficiently high temperatures to cause irreversible damage to the targeted tissue. However, this approach is prolonged, costly, and demands magnetic resonance thermometry or computed tomography to ensure that the intended area is effectively treated while minimizing damage to surrounding healthy tissue [37,38]. Additionally, thermal diffusivity can contribute to unintended harm to healthy tissue surrounding the target area [39].

Alternatively, histotripsy is a noninvasive and nonthermal US surgery method that utilizes short, high-intensity focused US pulses for noninvasive mechanical ablation, fractionating targeted soft tissue into subcellular debris through cavitation. Histotripsy relies on the controlled creation of acoustic cavitation leading to tissue breakdown. Both simulation and experimental evidence support the existence of nanometer-scale gas pockets within tissue that serve as cavitation nuclei when microsecond-length pulses reach peak negative pressures (PNP) surpassing an intrinsic threshold. Ex vivo experiments have determined this threshold to be in the range of 26–30 MPa for water-based tissues such as blood clots, liver, heart, brain and others [6]. While histotripsy can be employed for the treatment of various medical conditions, including tumors and other pathological tissues, safety concerns arise due to the necessity of focusing high energy into the body, potentially leading to off-target

effects [40,41]. Moreover, the motion caused by respiration can result in incomplete ablation or collateral damage, significantly compromising precision and efficacy [42]. Additionally, the requirement for manufacturing high-intensity focused transducers poses a challenge, adding to the technological limitations of the procedure [43]. In an attempt to decrease the pressure threshold needed for histotripsy, research was made to combine histotripsy with microbubbles (MB) or nanodroplets. However, within the megahertz US range, this combination led to only a 2- to 3-fold reduction in the onset pressure, still maintaining a relatively high pressure at approximately 10 MPa [44–47]. MBs are gas-filled bubbles that can be injected into the body and are typically on the order of micrometers in size. MBs were originally developed to serve as contrast agents and enhance the visibility of blood vessels and tissues. They have emerged as promising agents for various medical treatment applications. These contrast agents often composed of lipid or protein shells, exhibit unique acoustic properties that make them ideal for US-mediated therapies. MBs can be injected locally or into the bloodstream and, when exposed to US waves, these agents oscillate, producing localized effects. This phenomenon has been harnessed for targeted drug delivery, tumor ablation or blood brain barrier opening. The versatility and biocompatibility of MBs make them a compelling tool for innovative and minimally invasive treatment strategies [48–50]. In the drug delivery field, focused US therapy represents also a dynamic and multidisciplinary field that has garnered significant attention for its promising applications. A specific focus of investigation centers on sonoporation that refers to the temporary permeabilization of cell membranes induced by US waves. This technique utilizes acoustic energy to create transient pores in cell membranes, allowing for the enhanced delivery of therapeutic agents, genes, or other substances into the targeted cells [51]. This phenomenon can be facilitated by the oscillation of MBs or nanobubbles (NBs), another contrast agent used in US imaging, in response to US [52,53]. This approach is a promising targeted, non-viral, and non-toxic method for delivering genes and drugs and leverages the advantages of US (such as safety, ease of use, cost-effectiveness, and widespread clinical availability) [54,55]. The noninvasive characteristics of US allow direct application to deep-seated organs with site-

specific precision, facilitating sonoporation of deep tissues while minimizing off-target effects [56].

1.2 Objectives and significance of the research

Our research challenges the conventional notion that MB oscillations reach their peak around their resonance frequency (2–10 MHz). We observed that when stimulated at a frequency of 250 kHz, MB oscillations experience significant enhancement, as depicted in Figure 1. This phenomenon, identified as the Blake threshold effect, leads to substantial expansion of MBs well below their resonance frequency. In the presence of quasistatic pressure changes (excitation well below the natural resonance frequency), MBs demonstrate a rarefactional pressure threshold referred as the Blake threshold. Beyond this threshold, conditions of unstable equilibrium emerge due to the incapacity of MBs in the liquid to withstand excessively high static tension caused by rarefactional pressure [57]. Based on this initial discovery, our research goals are to develop a low energy cancer therapy platform using a combination of gas-bubbles and low frequency US, with a specific focus on tumor ablation and sonoporation. The specific aims are as follows:

Aim 1: Develop a low-energy US surgical method utilizing intratumorally injected MBs combined with low-frequency US.

Aim 2: Establish a noninvasive US surgical method using intravenously injected NBs combined with low-frequency US.

Aim 3: Create a platform for noninvasive drug delivery using NBs combined with low-frequency US.

In the realm of tumor ablation, the initial phase of the research entails utilizing MBs and intratumoral injection to establish a low energy histotripsy approach for cancer [58]. In the subsequent phase, we intend to develop a noninvasive therapeutic platform employing NBs, which can accumulate in the tumor post systemic injection. Upon accumulation within the tumor, coupled with low-frequency excitation, we aim to use NBs as mechanical therapeutic agents for histotripsy at a significantly lower cavitation threshold [59]. Simultaneously, the research aims to enhance drug delivery by poking large holes in cell membranes by leveraging the large oscillations of NBs following low-frequency

excitation [53]. The integration of NB and low-frequency US for cancer cell sonoporation is another course for noninvasive cancer therapy that can be synergized with the techniques that were developed in the previous aims to reduce tumor burden and facilitate drug delivery as a joint strategy for cancer treatement. Overall, these objectives involve refining and expanding the applications of focused US surgery through histotripsy and sonoporation. Challenges such as off-target effects, transducer fabrication, and the high energy required are addressed to reduce pressure thresholds and enhance safety. The exploration of low-frequency focused US introduces possibilities for noninvasive cancer treatment with clinical applicability [60,61]. The project encompasses theoretical predictions of gas bubble oscillations, tissue-mimicking experiments for optimization and multi-parameter evaluation, in vitro experiments with breast cancer cell suspensions, and in vivo experiments using a breast cancer tumor model in mice. The utilization of low-frequency US is particularly significant, as it aids in focusing through the human skull with minimal distortion and attenuation, crucial for brain therapy applications that could be tested in the future [29,40]. This technology provides essential tools for the noninvasive treatment of cancer, potentially revolutionizing health outcomes and offering minimally invasive approaches with applications across various biomedical domains.

1.3 The research structure

The research investigates the effect of low frequency US on gas bubbles, particularly MBs and NBs, as a platform for low-energy US therapy for tumors. MBs and NBs, composed of a gas core and stabilizing shell, play a pivotal role in US applications, offering a versatile tool in medical imaging and therapeutic platforms [49,62]. These agents enhance US imaging by providing contrast against surrounding tissues. When exposed to US waves, these contrast agents undergo oscillations, producing detectable acoustic signals that improve the visibility of blood vessels and enhance the delineation of structures in real-time imaging [63]. Beyond their imaging capabilities, these contrast agents are increasingly employed for therapeutic applications [64]. MB oscillations depend on US parameters; at a low acoustic pressure, MBs are compressed and expanded repeatedly in a process termed stable cavitation [65]. At higher

acoustic pressure MB undergoes inertial cavitation; the MBs disintegrate and fragment into smaller parts. Inertial cavitation produces a high level of energy, inducing liquid jets that can lead to acute mechanical damage to the surrounding environment [66].

Our research group recently revealed that in contrast to the common assumption that MBs oscillations peak around their resonance frequency (2–10 MHz), when they are stimulated at a frequency of 250 kHz, their oscillations are significantly enhanced (Figure 1). This phenomenon, known as the Blake threshold effect, triggers substantial MB expansion well below their resonance frequency [57]. In the first paper, we propose leveraging this increased MB expansion at low frequencies for localized fractionation of tumor cells. Beyond the improved vibrational response of MBs, utilizing low transmission frequencies offers advantages such as increased penetration depth due to reduced tissue absorbance at this frequency range, minimizing attenuation compared to higher frequencies and intracranial penetration ability [29]. Additionally, the lower frequency expands the focal zone, facilitating the simultaneous treatment of larger volumes and low-frequency US systems are more clinically accessible and cost-effective compared to high-frequency systems [57]. This accessibility is crucial for widespread adoption in medical settings.

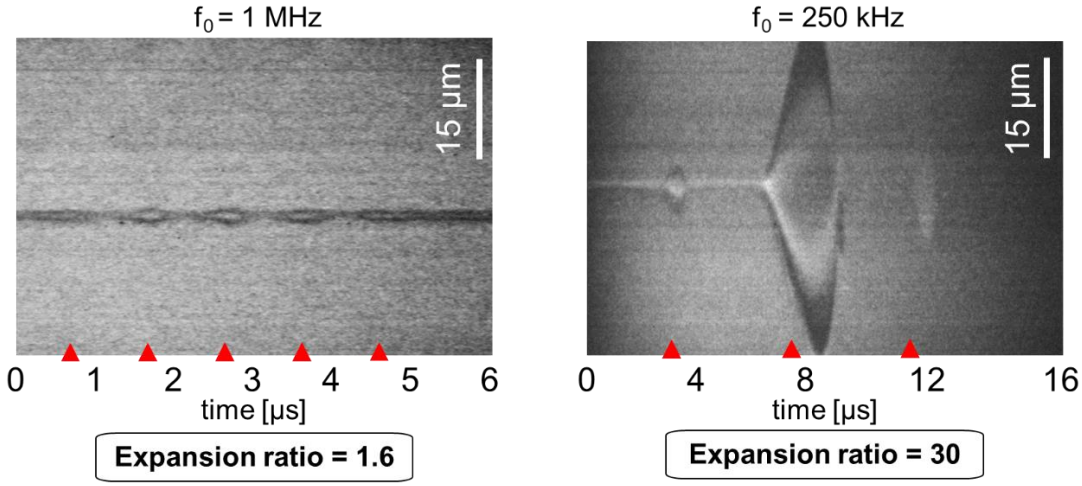

Figure 1: Effect of low frequency ultrasound on microbubbles oscillations. Ultra high-speed camera streak images of oscillating MBs with a resting radius of 1.5 µm for a peak negative pressure of 400 kPa at a center frequency of 1 MHz and 250 kHz [57].

We demonstrate that under low-frequency excitation (250 kHz and 80 kHz), high-amplitude MB oscillations occur at substantially lower pressures compared to higher MHz ultrasonic frequencies. For instance, inertial cavitation of MBs initiated at a PNP of 75 kPa only for a center frequency of 80 kHz and at a PNP of 180 kPa for a center frequency of 250 kHz. Utilizing low-frequency insonation of targeted MBs, we achieved low-energy tumor cell fractionation at pressures below a mechanical index (MI) of 1.9, in accordance with Food and Drug Administration (FDA) guidelines for imaging US applications. The US MI is a crucial parameter in US applications, providing a measure of the potential bioeffects associated with acoustic exposure. Represented by a dimensionless number, the MI takes into account both the peak rarefactional pressure and the square root of the center frequency of the US wave. This index serves as an indicator of the likelihood of cavitation in a liquid medium. In diagnostic applications, maintaining a low MI is generally preferred to minimize the risk of inducing cavitation and associated bioeffects, ensuring the safety of the imaging procedure [67,68]. We showcased in this work the ablation capabilities of the targeted MBs when combined with low frequency US at MI below 1.9 in vitro on breast cancer cells and in vivo in a breast tumor mice model. This innovative approach triggered powerful mechanical effects within tumors, dramatically reducing the requisite pressure for standard histotripsy procedures by over an order of magnitude. However, the relatively large diameter of MBs ranging from 1.5 to 4 μm limits their penetration into tumor tissue following systemic injection and necessitate intrusive intratumoral injections for tumor therapy purpose, maintaining the challenge of achieving noninvasive mechanical US surgery with low energy and optimal precision [69].

Addressing these limitations, in our second publication we present a noninvasive approach for low energy mechanical ablation of tumors that doesn’t require intratumoral injection. Although the delivery of particles up to 700 nm has been documented, achieving efficient transvascular passage from the bloodstream to the tumor interstitial space necessitates the use of particles smaller than 400 nm [70,71]. Therefore, here we introduce a therapeutic platform integrating systemically injected nanoscale NBs, having an average size of 180 nm, with low-frequency US. This novel combination enables remote,

low-energy mechanical US surgery for tumors in a noninvasive way. This noninvasive approach is facilitated by the capability of NBs to effectively penetrate tumors after a systemic injection, leveraging the leaky tumor vasculature and taking advantage of the enhanced permeability and retention (EPR) effect [72]. Due to their size and their main use as contrast agents in imaging, NBs are commonly paired with high US frequencies, typically in the tens of megahertz range, corresponding to their resonance frequency [73]. The resonance frequency is defined as the frequency at which the bubble's first harmonic response reaches a local maximum, estimated at 40 MHz for a 200 nm NB [74]. However, at this frequency, substantial oscillations of NBs at high amplitudes are not observed, thereby constraining their capacity to induce significant bioeffects through cavitation [75]. We demonstrate that the Blake threshold effect can induce intense NBs oscillations, making them viable as low-energy cavitation nuclei for histotripsy. We theorize that the Blake threshold is applicable to any gas-bubble excitation well below its resonance frequency. Given that the resonance frequency of NBs is higher than that of MBs, exciting NBs in the same kilohertz range as MBs will result in strong NBS oscillations triggering potent mechanical effects in tumors following systemic injection.

The research compares the acoustic response of MBs and NBs after insonation at frequencies of 250 or 80 kHz and reveals that higher pressures are required to implode NBs compared to MBs. Complete NBs destruction is achieved at a MI of 2.6 for 250 kHz insonation vs. 1.2 for the 80 kHz frequency, demonstrating compliance with safety regulations recommending operation below a MI of 1.9. In vitro, in breast cancer tumor cells, cell viability is significantly reduced proving the ability of NBs to reach major bioeffects. In vivo, in a breast cancer tumor mice model, NB tumor distribution and accumulation are demonstrated using fluorescence microscopy and US imaging. Ultimately, NB-mediated low-frequency insonation of breast cancer tumors results in effective mechanical tumor ablation and tumor tissue fractionation. Our research unveils the pivotal role of NBs as noninvasive therapeutic tools, generating potent mechanical effects within tumors following systemic injection when coupled with low-energy insonation at an 80 kHz frequency, significantly below the NB resonance frequency.

In the third paper, based on the large NBs oscillations obtained at low frequency US, we explore their potential for poking large holes in cancer cell membranes and facilitating drug delivery as a complementary approach to histotripsy for tumor therapy. In the context of cancer therapy, it is necessary to concurrently attain significant delivery efficacy of therapeutic agents and decrease cell viability. This dual objective is critical as reducing the tumor burden is crucial to the success of cancer treatment [36]. In this study, we demonstrate that coupling NBs with low-frequency US achieves high-amplitude oscillations, enabling low-energy sonoporation of cancer cells. The method was fine-tuned for the delivery of four fluorescent molecules ranging from 1.2 to 70 kDa to breast cancer cells, with results compared to targeted MBs. Optimal PNP varies between 300 and 500 kPa depending on the fluorescent molecule size. These results are comparable to targeted MB-mediated sonoporation, indicating that NBs can serve as noninvasive sonoporation agents with similar potency, despite their reduced size. Furthermore, NBs effectively reduce cell viability, suggesting their potential to diminish tumor burden, a critical aspect of successful cancer treatment. This method presents a noninvasive, low-energy tumor sonoporation theranostic platform that can be synergistically combined with other therapies to maximize therapeutic benefits in cancer treatment or applied in gene therapy applications.

In summary, our research introduces a pioneering advancement in the realm of US therapy for tumors, focusing on the impact of low-frequency insonation on gas bubbles, particularly MBs and NBs. The study unveils a notable finding: the expansion of both MBs and NBs demonstrates a non-linear increase in response to pressure reduction when the center frequency excitation is lowered. This phenomenon can be harnessed for low-energy mechanical ablation and sonoporation applications with a reduction in the required pressure by an order of magnitude compared to conventional US therapy approaches, highlighting the potential for more efficient and less invasive treatments. Notably, the incorporation of NBs in the study enables noninvasive therapeutic applications, signifying a significant leap forward in the development of advanced and patient-friendly treatment modalities. Overall, the findings offer a comprehensive understanding and application of gas bubbles in US therapy,

paving the way for innovative and minimally invasive approaches in cancer treatment.

1.4 Methods

1.4.1 Ultrasound Setup

The experimental therapeutic configuration comprises a 64-mm-diameter spherically focused single-element transducer (H117 or H115) positioned at the bottom of a degassed and deionized water tank, facing upward and focused to a distance of 45 mm. The fundamental frequency for these transducers is 250 kHz. Notably, both H115 and H117 transducers are equipped to support center frequencies of both 250 and 80 kHz through custom matching networks from Sonic Concepts. The transducer transmits a sinusoid at the specified frequency, and the waveform is generated using a transducer power output unit that combines an arbitrary waveform generator with a radiofrequency amplifier (TPO-200, Sonic Concepts). When employing the 80 kHz matching network, the bandwidth ranges from 70 kHz to 105 kHz. At 80 kHz, one-third of the maximal PNP is achieved compared to the maximal pressure when operating at the center frequency of the transducer (250 kHz). Beam pattern measurements using a calibrated hydrophone (NH0500) reveal a focal width of 18.9 mm and a focal length of 92.7 mm for the 80 kHz center frequency configuration, while the focal width and focal length are 7 mm and 50 mm, respectively, for the 250 kHz center frequency.

In each experiment, the intended target was positioned at the focal spot. For characterization experiments involving NBs and MBs in tissue-mimicking phantoms, an agarose phantom containing an inclusion was filled with the NB/MB suspension. In in vitro ablation and sonoporation experiments, a 0.5 mL Eppendorf tube containing breast cancer cells was used. Finally, for in vivo experiments, a mouse was positioned such that the breast cancer tumor was located precisely at the focal spot of the transducer.

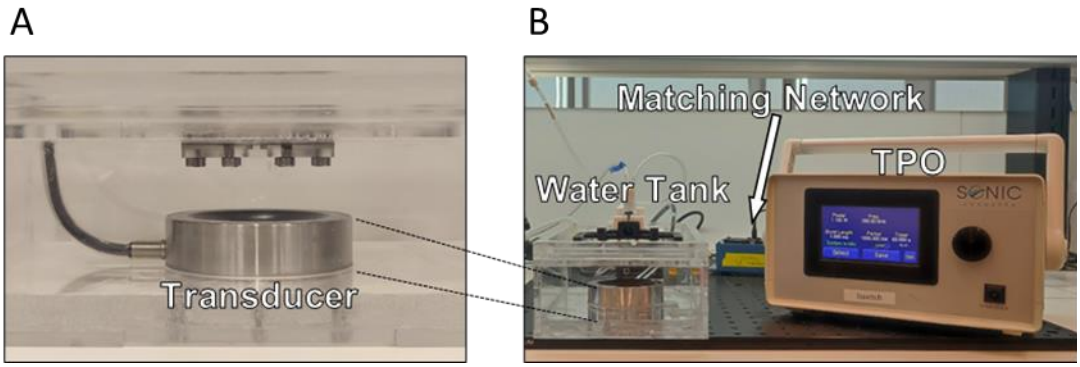

Figure 2: Therapeutic ultrasound setup. A) H115 single element therapeutic transducer positioned at the bottom of a degassed and deionized water tank. B) The complete ultrasound setup comprising the transducer power output unit that combines an arbitrary waveform generator with a radiofrequency amplifier, the matching network and the water tank with the therapeutic single element transducer.

1.4.2 Hydrophone calibrations

To assess the pressure produced by therapeutic US transducers, calibration was performed using a calibrated wide-band needle hydrophone (NH0500, Precision Acoustics, Dorchester, UK) with an active aperture of 0.5 mm in a degassed and deionized water tank. The hydrophone probe, mounted on a three-dimensional positioning system (Newport motion controller ESP301, Newport 443 series), was positioned perpendicularly to the emitted field. The acoustic pressure fields transmitted by the therapeutic transducers (H117 or H115, Sonic Concepts, Bothell, WA, USA) were captured at the focal spot using a digital oscilloscope (MDO3024, Tektronix, OR, USA), and the PNP was extracted from each measurement to construct a calibration curve for the therapeutic transducer. PNP Calibration was conducted at both transmitted frequencies (80 and 250 kHz), and the frequency content was verified by transmitting a single-cycle signal. The data recorded by the hydrophone were stored, and the resulting spectrum was subjected to analysis.

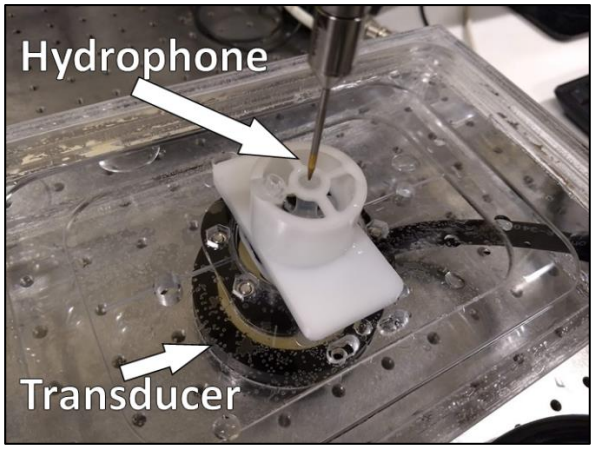

Figure 3: Pressure calibration of H115 transducer. Calibration was performed using a calibrated hydrophone immerged in degassed water and positioned at the focal spot of the therapeutic transducer.

1.4.3 Tissue mimicking phantoms experiments

Agarose powder (A10752, Alfa Aesar, MA, USA) was mixed with deionized water to create a 1.5% solution at room temperature, heated until complete powder dissolution, and then poured into a 3D printed custom mold. The mold featured a 6 mm rod inclusion designed to contain MBs or NBs solutions. The resulting phantom was cooled at room temperature. The phantom was placed at the focal spot of the US setup previously described. In each tissue mimicking phantoms experiment, a mixture of MBs, targeted MBs bound to cells or NBs were diluted in degassed phosphate buffered saline (PBS) and injected into the rod inclusion.

A programmable US system (Verasonics, Vantage 256, Verasonics Inc., Redmond, WA, USA), was utilized to image the tissue-mimicking phantom before and after applying low-frequency therapeutic US. The linear L7-4 imaging transducer (Philips ATL), controlled by the Verasonics system was placed perpendicular to the spherically focused therapeutic transducer and US imaging in standard two-way focusing and focused to a depth of 13 mm was performed at a center frequency of 5 MHz with an excitation of 1 cycle for each transmitted pulse. The transducer has 128 elements, with an element size of 7 mm × 0.283 mm (height × width) and a kerf width of 0.025 mm. B-mode images of the NB/MB/targeted MB filled inclusion were acquired by the imaging transducer before and after the application of low-frequency therapeutic US (250 and 80 kHz). Images contrast, defined as the difference in brightness

before and after therapeutic US treatment at the specified region of interest were calculated (eq 1):

$$Contrast[dB] = 20\ \log_{10}\left(\frac{u_i}{u_0}\right)$$

where μ_i represents the mean of the rod inclusion area after US insonation, and μ_o designates the mean of the same region before US treatment. In each tissue-mimicking experiment, a solution containing 3.75×10^9 NBs diluted in 300 µl of degassed PBS, was injected into the rod inclusion within the agarose mold. For MBs experiments, 3×10^6 MBs, diluted in 300 µl of degassed PBS, were utilized. These concentrations result from concentration optimizations experiments. The low-frequency therapeutic insonation consisted of a 125-cycle sinusoid with a 250 kHz or 80 kHz center frequency and a pulse repetition frequency (PRF) of 30 Hz, unless specified otherwise. Details regarding PNP and treatment time duration were provided in the relevant sections of the articles.

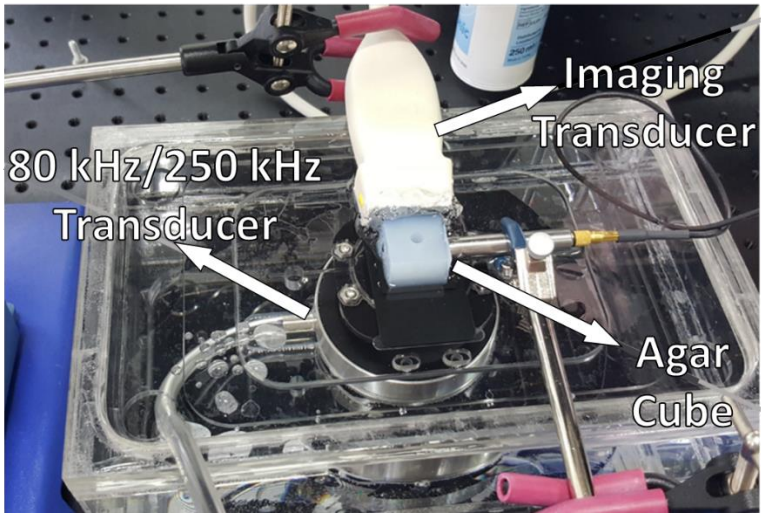

Figure 4: Tissue mimicking phantoms setup for bubbles oscillations characterization. The tissue mimicking phantom was placed at the focal spot of the US therapeutic transducer and filled with micro- or nano-bubbles. Imaging transducer was utilized to image the tissue-mimicking phantom and evaluate micro- and nano-bubbles inertial cavitation.

1.4.4 Sonoporation experiments

The delivery to 4T1 breast cancer cells [76] of a range of fluorescent molecules with sizes from 1.2 kDa to 70 kDa was investigated. 7-aminoactinomycin D (7-AAD, Thermo FisherScientific, A1310) with a molecular weight of 1.2 kDa and

fluorescein isothiocyanate–dextran molecules with average weights of 4 kDa (FITC-Dextran 4, 46944, Sigma-Aldrich), 20 kDa (FITC-Dextran 20,Sigma-Aldrich, FD20), and 70 kDa (FITC-Dextran 70, Sigma-Aldrich, 46945) were used for sonoporation at concentrations of 5 μg/ml for 7-AAD or 1 mg/ml for FITC-dextran. Due to the spatial characteristics of the transducer's focal spot, the experiments were conducted within Eppendorf tubes. For the 250 kHz center frequency, the full width at half maximum for the lateral and axial axes was 7 × 50 mm. The elongated shapes of both the Eppendorf tubes and the focal point were strategically utilized for the treatment within these tubes. This approach facilitated the simultaneous treatment of the entire volume without the need for mechanical transducer movement, which would have been necessary if adherent cells in plates were used. Although the initial cell culturing took place in plates, after undergoing US treatment, the cells were transferred back to the 24-well plates. The control groups followed identical procedures to the treated groups throughout the experimental process.

A mixture of 2.5 x 10^5 cells, sonoporated fluorescent molecules and NBs, MBs or targeted MBs at various concentrations was transferred to 0.5 mL Eppendorf tubes. Following that, degassed PBS containing calcium and magnesium (PBS+/+) was added to achieve a final volume of 0.48 mL, and a 250 kHz US treatment was applied to the tubes using the previously described low-frequency US setup, with a PRF of 30 Hz and a 0.5 ms burst length. In the 7-AAD and FITC-Dextran 4 kDa experiments, US treatment occurred immediately after adding the fluorescent material to the 0.5 ml Eppendorf tube to prevent undesirable cellular uptake due to the molecules' small size.

The first molecule investigated in this study was 7-AAD (1.2 kDa). 7-AAD is a dye impermeable to membranes that undergoes a spectral shift upon binding to DNA. In the 7-AAD sonoporation experiments, after US insonation, Hoechst (33342, Abcam) was added to the tube to enable total cell counting of the sample (at a concentration of 10 μg/ml). The suspension was then transferred to a 35 mm cell culture dish (430165, Corning) and examined under a fluorescence microscope (10× magnification). Imaging included bright field, a DAPI filter, and a mCherry filter. For analysis, a total of seven images were captured from different locations within the culture dish.

Unlike 7-AAD, which generates a fluorescent signal only from stained cells and does not introduce background fluorescence in the suspension, FITC-dextran has inherent fluorescence, leading to a high background signal immediately after treatment. To address this issue, after US sonoporation, the cells were transferred to a pre-prepared 24-well plate (3526, Corning) filled with 300 µl of complete culture media (2.5% penicillin−streptomycin). The plate was then placed in a humid 5% CO_2 incubator and incubated at 37 °C for 24 hours enabling cells to adhere to the plate. Each well was then thoroughly rinsed three times with PBS+/+ to remove non-delivered FITC molecules, eliminate any lingering fluorescent background signal and non-viable cells, which did not adhere and remained in the suspension. Complete media was then added and cellular uptake and viability were visualized and quantified using the IncuCyte Live-Cell Analysis System (Essen Bioscience). The presented process makes the FITC-delivery experiments an accurate measure to assess cell viability and molecular uptake. Each group's experiments were performed in triplicate.

For NB optimizations experiments, a consistent treatment duration of 30 seconds was administered, which was optimized in a previous study [59]. Concentrations tested ranged from 1.29×10^7 NBs/µL (1X) to 2.06×10^8 NBs/µL (16X). Control groups included a sham group, Free MB (mixed) + US at a concentration of 50 MB/cell, US treatment only, and NB only (using the optimal NB concentration of 1.55×10^8 NBs/µL). In free MB experiments, the MB suspension was mixed immediately before US application to increase the proximity between the MB and the cells. This step was added due to the MB propensity to float. In FITC 4 kDa, 20 kDa, and 70kDa sonoporation experiments, the targeted MBs were added to the cell mixtures at a concentration of 50 targeted MB/cell.

To analyze the 7-AAD sonoporation experiments, ImageJ software was used. Each microscope image was uploaded, the image type was converted to 16-bit, the threshold was adjusted to enhance the visibility of the stained cells and remove the background. Each experiment was performed in triplicate, with a total of 7 images captured in each repetition, resulting in 21 images analyzed for each group. The fraction of fluorescent cells was determined by calculating the percentage of 7-AAD-stained cells (red) divided by the total number of cells

(Hoechst-blue-stained cells). The FITC sonoporation experiments were analyzed using the IncuCyte Live-Cell Analysis System. For each well, sampling was carried out 25 times at a magnification of 20×. The calculation involved normalizing the green confluence (green cell area) by the phase confluence (total cell area). GraphPad Prism 9 software was utilized for statistical analysis. Significance was determined for P values <0.05, adjusted for multiple comparisons as specified in the figure captions. The results are presented as the mean ± SD.

1.4.5 In vivo ultrasound experiments

A total of 80 bilateral FVB/NHan®Hsd breast tumor-bearing mice were included in the in vivo study. To obtain this model, the Met-1 mouse breast carcinoma cells [77], obtained from Prof. Neta Erez (Tel Aviv University, Tel Aviv, Israel), were injected into female FVB/NHanHsd mice aged 8 to 12 weeks (Envigo, Jerusalem, Israel). The cells were cultured in Dulbecco modified Eagle medium (DMEM, high glucose) supplemented with 10% v/v fetal bovine serum, 1% v/v penicillin–streptomycin, and 0.11 g/L sodium pyruvate at 37 °C in a humidified 5% CO_2 incubator. On the day of injection, Met-1 cells were collected using TrypLE Express dissociation reagent (Gibco Corp, 12604-013, GrandIsland, NY, USA), reaching a final concentration of 1×10^6 cells in 25 µL PBS+/+. Subsequently, these cells were subcutaneously injected into the #4 and #9 inguinal mammary fat pads. Anesthesia was induced using 2% isoflurane in ambient air (180 mL/min, SomnoFlo, Kent Scientific). Tumor size was monitored every 4 days until reaching approximately 4 mm in diameter, which occurred around 14 days after cell injections. All animal procedures adhered to ethical guidelines and were approved by the Institutional Animal Care and Use Committee (IACUC) of Tel Aviv University (IACUC Protocol #01-20-037).

MB-mediated ablation: Mice were positioned on their side atop an agarose pad, ensuring the tumor was precisely located at the transducer's focal spot, with US gel used for effective coupling. The area to be treated was shaved, and additional fur was removed using a depilatory cream to enhance coupling. To prepare the agarose spacer, agarose powder (Alfa Aesar, MA) was mixed with deionized water to form a 1.5% solution at ambient temperature. The mixture was heated until all powder dissolved, poured into a custom mold, and allowed

to cool at ambient temperature. Before initiating the ablation treatment, a freshly prepared solution containing 2×10^7 targeted MBs in 20 µL degassed PBS was intratumorally injected. The injection was performed immediately before each treatment session. The 250/80 kHz spherically-focused single-element transducer was positioned at the bottom of a degassed water tank, facing upwards and aligned to focus the agar spacer. The agar spacer, created in a custom mold, was designed to place the tumor at the transducer's focal depth (z = 45 mm). For treatments with center frequencies of 250 and 80 kHz, a PNP of 800 kPa (MI of 1.6) and 250 kPa (MI of 0.9) were applied, respectively. The parameters were selected to maintain a similar Cavitation Index (CI) for both frequencies, approximately ~3.2, while ensuring that the MI remained below the guideline of 1.9. In both cases, a 125-cycle sinusoidal US signal with a PRF of 30 Hz and a total duration of 1 minute was employed. The distribution of targeted MBs within the tumor before and after treatment was evaluated using US imaging on the Vevo 2100 US system (Visualsonics, Canada). Control groups included Non-Treated Control (NTC), targeted MBs only (without US treatment), and US only. Bilateral tumor-bearing mice were euthanized one day after US-mediated ablation for tumor removal. Tumors were covered in Leica OCT cryocompound ‘tissue freezing medium’ (Leica Microsystems, Bensheim, Germany) and flash-frozen in 2-methylbutane (Sigma-Aldrich) using liquid nitrogen. The tumors were then transferred to a -80º refrigerator until sectioning. Leica CM1950 Cryostat (Leica Biosystems Inc) was used to cut the tumors into 12 µm slices, which were mounted on microscope slides and placed in dark slide boxes for air-drying at room temperature. Slides were stained with hematoxylin (Leica 3801542) and eosin (Leica 3801602) (H&E) following a standard procedure. The H&E slides were scanned using the Aperio Versa 200 slide scanner (Leica Biosystems, Buffalo Grove, IL) at 20x optical magnification.

NB tumor distribution experiments: For the NB tumor distribution imaging experiments, we utilized a high-frequency US transducer (L22-8v, Verasonics, USA) controlled by the Verasonics programmable US system. Contrast pulse sequence mode with coherent compounding was implemented by sending three successive single-cycle pulses (+1/2, -1, +1/2). Additionally, coherent compounding was achieved by transmitting plane waves at three different

angles (−5°, 0°, 5°), with one full frame being the combination of the nine transmit/receive events. The transmitted center frequency was 10 MHz. Prior to NB injection, we acquired the baseline signal of the tumor core. Subsequently, $6.6x10^{11}$ NBs in 200 µl of PBS were systemically injected, and the tumor was periodically imaged for 10 minutes post-injection. To validate the existence of tumor-accumulated NBs, we performed, 10 minutes after NB injection, cardiac perfusion with 15 ml of degassed PBS through the left ventricle to eliminate non-extravasated NBs within the blood vessels. The perfused tumors were then collected and subjected to imaging using contrast harmonic US imaging. After perfusion, we extracted the tumors and performed US imaging to detect the signal produced by the NBs that had accumulated within the tumor tissue. The extracted tumors were then exposed to an 80 kHz center frequency US, using an MI of 1.3, a burst length of 1.56 ms, a PRF of 30 Hz, and a total treatment duration of 2 minutes. Subsequent to the US treatment, imaging was performed using the aforementioned contrast pulse sequence mode to evaluate the US signal within the tumor. Sham tumors underwent cardiac perfusion without NB injection, followed by US imaging of the perfused tumors. NB extravasation in the heart, kidney, liver, and spleen was assessed under similar conditions. NBs were systemically injected and allowed to circulate for 10 minutes before cardiac perfusion as previously described. Heart, kidney, liver, and spleen were then collected and imaged using contrast pulse sequencing imaging. Sham organs underwent cardiac perfusion without NB injection, followed by US imaging of the perfused organ.

For the evaluation of fluorescent NBs tumor extravasation, in-vivo experiments involved three groups of mice: sham, fluorescent MBs, and fluorescent NBs. Either $6.6x10^{11}$ fluorescent NBs in 200 µl or a volume of 50 µl containing $2x10^{7}$ fluorescent MBs were systemically injected and allowed to circulate for 10 minutes. 10 minutes post-injection, cardiac perfusion was performed to wash the bubbles from circulation, and the tumors were harvested. They were covered in Leica OCT cryocompound and flash-frozen in 2-methylbutane using liquid nitrogen. The tumors were then transferred to a -80º refrigerator until sectioning. Leica CM1950 Cryostat was used to cut the tumors into 12 µm slices, which were mounted on microscope slides and placed in dark slide

boxes for air-drying at room temperature. Microscopy imaging was performed within 1 hour from sectioning, using an upright microscope (Olympus BX63) with an excitation wavelength of 615 nm and microscope objectives of 4x and 20x. Statistical analysis of fluorescence was conducted for the three different groups, with fluorescence quantification carried out on the 20x magnification microscopy images in ImageJ.

NB-Mediated Ablation: Systemic injection of $6.6x10^{11}$ NBs in 200 µl or a volume of 50 µl containing $2x10^{7}$ MBs was administered. 10 minutes post-injection, an 80 kHz US treatment was applied to the tumor, employing a MI of 1.3, a burst length of 1.56 ms, a PRF of 30 Hz, and a total treatment duration of 2 minutes. Control groups included a sham group and US alone. Mice were sacrificed 24 hours after treatment for tumor extraction and histological analysis. Histological assessments were conducted using both frozen and paraffin-embedded tumors. Tumors were frozen as previously described, cryo-sectioned into 12-µm-thick slices and stained with H&E following standard procedures. The slides were then scanned with the Aperio Versa 200 slide scanner at 20× optical magnification. For a detailed examination of tumor structure and cell morphology, tumors were also paraffin-embedded, and 4 µm sections were stained with H&E. For paraffin embedding, tumors were extracted, fixed in 10% natural buffer formalin at 4 °C for 24 hours, and subsequently paraffin-embedded. Tissue sections were deparaffinized in a xylene ethanol gradient and stained using the standard H&E procedure for evaluating tissue damage. ImageJ was utilized for post-processing of images to compare and quantify the damage, specifically the lesions generated in the samples across different groups. In the case of major internal organs (heart, kidney, liver, spleen, and lung) histology following NB-mediated ablation treatment of breast cancer tumors, mice were sacrificed 24 hours post-treatment, and the organs were harvested and frozen for histological analysis. Organ tissues were cryo-sectioned into 12-µm-thick slices and stained according to the standard H&E procedure. The resulting slides were then scanned using the Aperio Versa 200 slide scanner at 20× optical magnification.

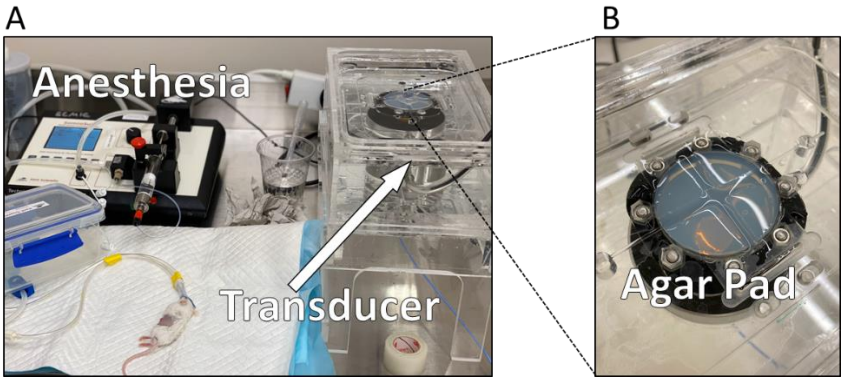

Figure 5: In vivo setup for ultrasound-mediated ablation. A) Anesthesia was induced on mice using an automated electronic vaporizer of isoflurane. Therapeutic transducer for treatment was positioned at the bottom of a degassed and deionized water tank. B) Agar pad was precisely located at the transducer's focal spot ensuring tumor positioning.

2. Articles

2.1 Article I:

Acoustically Detonated Microbubbles Coupled with Low Frequency Insonation: Multiparameter Evaluation of Low Energy Mechanical Ablation. Bioconjugate Chemistry (2021)

2.2 Article II:

Low frequency nanobubble-enhanced ultrasound mechanotherapy for noninvasive cancer surgery. Nanoscale (2022)

2.3 Article III:

Nanobubble-mediated cancer cell sonoporation using low-frequency insonation. Nanoscale (2023)

3. Additional results

3.1 Tumor spheroids as model for nanobubbles penetration evaluation

Tumor spheroids have emerged as an advanced 3D tumor mimicking model by encompassing a substantial extracellular matrix that closely mirrors the complexities of in vivo environments. This advanced model uniquely captures the dynamic interplay of spatial cell-cell interactions and establishes a gradient distribution of critical elements such as oxygen, nutrients, and metabolites within the spheroid structure, reproducing the intricate tumor microenvironment [78]. For our study, we utilized MET-1 cells derived from mouse breast carcinoma to construct the spheroids, ensuring a biologically relevant representation of breast cancer within the tumor microenvironment.

Briefly, the spheroid preparation custom process involves trypsinizing MET-1 cells, adjusting the concentration to 50,000 cells/ml and 2.5% of Matrigel (BD Biosciences, cat no356230). 100 µL of the cell-Matrigel mixture is transferred to each well of Ultralow attachment plates with U-well (round) bottom (Corning, cat no 7007). The plate is then centrifuged for 15 minutes at 2250 rpm. After 3 days, the spheroids are ready for use in subsequent experiments. Our primary objective in this study is to assess the capacity of NBs to penetrate breast tumor spheroids. To evaluate their penetration, we synthesized fluorescent NBs. The total fluorescence signal within the spheroid is anticipated to provide insight into the ability of these NBs to infiltrate the breast tumor spheroids. This comprehensive investigation, combining the construction of MET-1 cell-derived spheroids with the assessment of NB penetration, holds significant promise for advancing our understanding of nanomedicine applications within the specific context of breast cancer models. The detailed protocol ensures the reproducibility and reliability of our experimental setup, paving the way for innovative therapeutic interventions in the realm of breast cancer treatment.

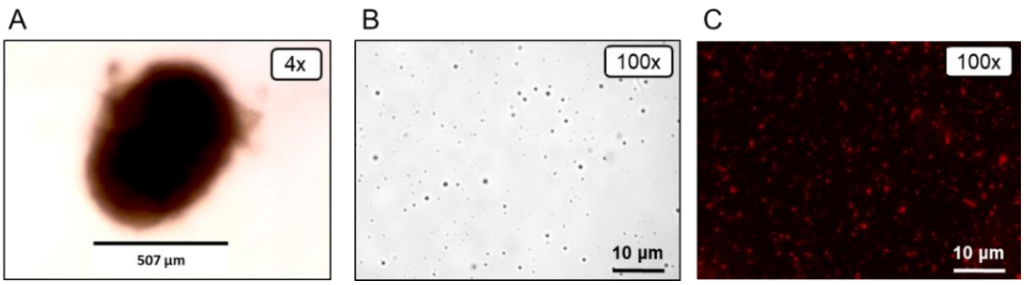

Figure 6: Tumor spheroids as model for nanobubbles penetration evaluation. A) Bright field image of breast cancer spheroid cultured under static condition for 3 days. B) Characterization of nanobubbles under a microscope. Bright-field images were acquired at 100X magnification. C) Characterization of DiI-nanobubbles under a fluorescent microscope. Images were acquired at 100X magnification. Scale bars are 10 µm.

3.2 Evaluation of tumor growth following microbubble-mediated histotripsy

We examined the effect of low energy targeted MB-mediated histotripsy on breast tumor growth on a tumor bearing mice model. Two weeks after inoculation of the model as described previously in the methods part, the tumors were treated by targeted MB intratumor injection and low frequency application of 1 minute at a center of frequency of 80 kHz and MI of 0.9; a 125-cycle sinusoidal US signal with a PRF of 30 Hz was employed. MET-1 tumor mice control groups comprised NTC group, targeted MB intratumoral injection only group and US only group. Targeted MB-mediated histotripsy ablation at pressures below a MI of 1.9, in accordance with FDA guidelines for imaging US applications significantly inhibited tumor growth without producing significant alterations in body weight.

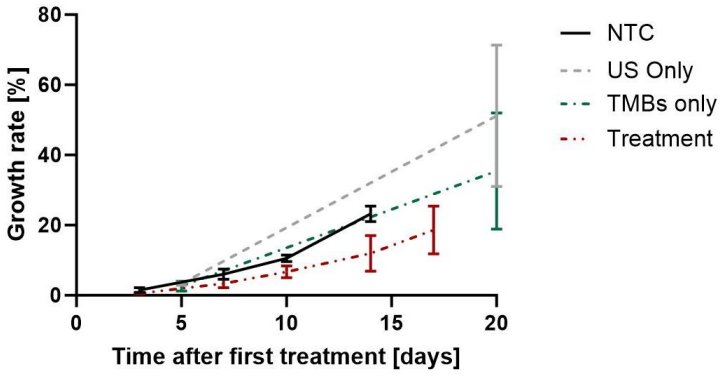

Figure 7: Tumor growth following targeted microbubble mediated ablation. FVB mice were inoculated with MET-1 orthotopic tumors, then treated with targeted microbubbles-mediated low energy histotripsy ablation on day 14. Control groups were no treatment control, targeted microbubbles intratumoral injection only and US only.

3.3 Combination of nanobubble-mediated histotripsy and chimeric antibody-based receptor T cells therapy

The application of chimeric antibody-based receptor (CAR) T-cell therapy in cancer treatment has shown remarkable success in achieving complete remission in pilot clinical trials for late-stage leukemia and lymphoma. However, the efficacy of CAR-T cell therapy in inoperable solid and metastatic tumors, a challenging domain, remains unaccomplished. Unlike hematological malignancies where CAR-T cells are systemically administered with easy access to the target, the application of CAR-T cells in solid tumors faces obstacles [79].

To overcome these challenges in solid tumors, we propose a novel approach combining NB-mediated low-energy histotripsy to enhance CAR-T cell infiltration, modify the tumor microenvironment, and ultimately improve therapeutic outcomes. This study focuses on evaluating the ability of NB-mediated low-energy histotripsy to enhance CAR T-cell therapy for breast tumors, providing a potential therapeutic benefit for human epidermal growth factor receptor 2 (HER-2) induced breast cancer.

The HER-2 transgenic mouse model, which overexpresses the human erbB-2 gene, serves as a valuable tool in this investigation. In this model, female mice express the transgene in all tissues, with spontaneously developing tumors limited to the mammary gland. This transgenic mouse model was developed by

the Anat Globerson Levin Immunology Research Laboratory at Ichilov Hospital. As a crucial initial step toward combining CAR-T cell therapy, our objective is to determine if NB-mediated histotripsy can effectively achieve significant tumor fractionation and potentially enhance CAR T-cell therapy using low-energy US. In experiments conducted 24 hours after NB-mediated histotripsy in the HER-2 transgenic mouse model, extracted tumors underwent cryosectioning for histological analysis. The results revealed effective tumor fractionation, cell loss, and hemorrhage at low US energy levels, providing promising insights into the feasibility of our proposed combination therapy.

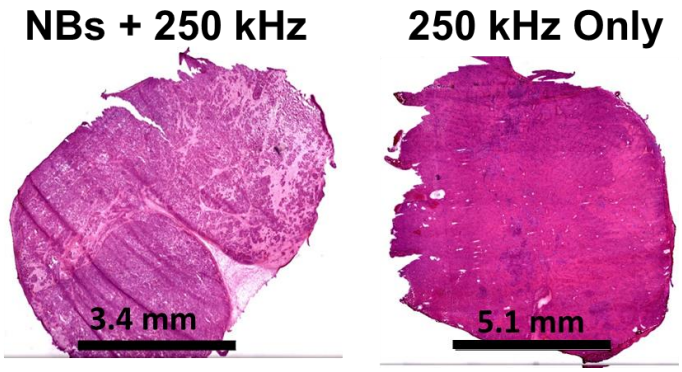

Figure 8: Nanobubble-mediated low frequency insonation of spontaneous human epidermal growth factor receptor 2-breast cancer tumors in vivo. Histological photomicrographs of tumor treated with nanobubbles and 250 kHz insonation and control tumor treated with ultrasound only. Frozen tumors were cryo-sectioned to 12 μm thick slices and stained with hematoxylin and eosin according to the standard procedure.

3.4 Evaluation of immune system response following nanobubbles mediated treatment and anti-PD1 injection

Tumor histotripsy treatments have demonstrated promising immunostimulatory effects, including the release of tumor-associated antigens, increased dendritic and macrophage cell infiltration, heightened CD8+ T-cell responses and suppression of distant metastases [80]. Our current objective is to evaluate the potential of our novel low-frequency US combined with NBs treatment in enhancing T-cell and macrophage cells infiltration while concurrently reducing tumor size. By utilizing US at 80 kHz in conjunction with NBs, we seek to achieve mechanical ablation, anticipating a more robust infiltration of cytotoxic T cells and macrophages. This approach will be complemented by checkpoint inhibition treatment (aPD-1), and the treatment response will be assessed

through measurements of tumor growth rate, immunohistochemistry staining to evaluate immune cell infiltration, and a survival study.

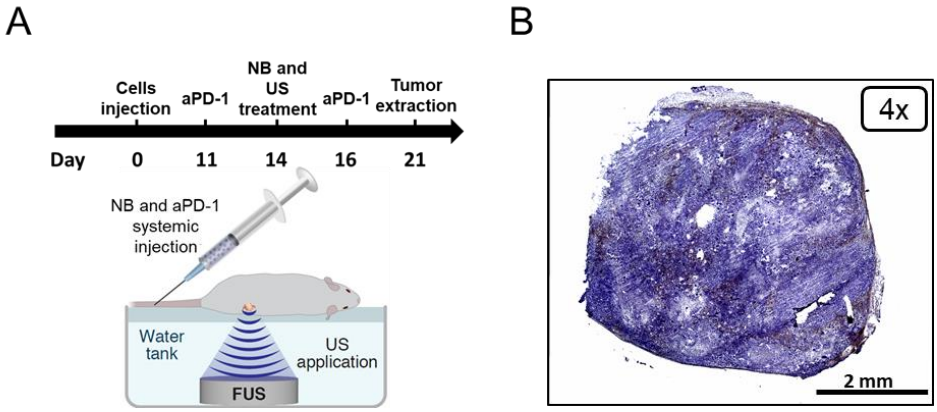

Figure 9: Evaluation of immune system response following nanobubbles mediated treatment and anti-PD1 injection. A) Schematic of the experiment timeline. The breast tumors are sized frequently before and during treatment. B) Immunohistochemistry staining image of breast tumor following NBs-mediated ultrasound treatment and aPD-1 injection. Positive immunohistochemical reactions (IHC -brown colour) indicate CD8+T cell infiltration into breast tumors.

4. Discussion

4.1 Summary

The field of US-based therapies for localized tumor treatment, serving as a non-invasive alternative to traditional approaches, is a growing field with significant clinical relevance. For instance, US-based ablation techniques offer advantages such as reduced pain, shorter recovery times, and the ability to treat patients ineligible for surgical resection due to factors like tumor location, age, or concurrent medical conditions [26,81,82]. The rapid advancement of imaging modalities and devices further enables US tumor ablation to be image-guided in many cases [25]. Another application in local tumor treatment is sonoporation, an expanding field that has demonstrated efficacy in delivering drugs and genes to various cell types and tissues. This method's advantages include cost-effectiveness, deep penetration, and widespread availability, distinguishing it from other delivery techniques. In comparison to biological methods like viral vectors, sonoporation enhances the spatiotemporal precision of gene delivery, significantly reducing undesirable side effects and non-specific toxicity [51].

The current research aims to assess the integration of micro- and nano-bubbles in combination with low-frequency US to enhance the efficacy and safety of histotripsy and sonoporation techniques for local tumor therapies. Two approaches for tumor fractionation via histotripsy are under evaluation. The first involves intratumoral injection of targeted MBs to establish a low-energy histotripsy approach for cancer. The second utilizes systemically injected NBs, with a mean diameter of 180 nm, for non-invasive tumor fractionation. For enhanced sonoporation application, NBs are employed, overcoming limitations associated with the larger MB diameter used in most sonoporation studies. To develop these methods, optimization of US specifications (center frequency, PNP, PRF, duty cycle, and treatment duration), bubbles formulation, and concentration is essential. The oscillations of MBs and NBs at 80 and 250 kHz were experimentally evaluated initially through phantom experiments to characterize their inertial cavitation behavior. These experiments aimed to assess, through experimental observation, the destruction of MBs and NBs as a function of PNP. The evaluation included the application of low-frequency insonation to an MB/NB-filled inclusion, while assessing the impact of insonation parameters on inclusion contrast using a dual imaging-therapy setup. This approach facilitates the multiparameter evaluation of insonation parameters and NB/MB concentrations.

The direct comparison of contrast reductions for NBs and MBs in relation to the MI at frequencies of 250 kHz and 80 kHz revealed that destruction occurred at a lower MI for the 80 kHz center frequency. For instance, a contrast reduction of over 20 dB was observed for MBs at 290 kPa (MI: 0.58) at 250 kHz and 120 kPa (MI: 0.42) at 80 kHz. Higher PNPs were necessary to achieve maximal contrast reduction for NBs compared to MBs at both frequencies. At 250 kHz, MBs reached maximal contrast reduction at 440 kPa (MI: 0.9), while complete NB destruction required 1300 kPa (MI: 2.6). Notably, NB maximal contrast reduction occurred at an MI of 2.6 for 250 kHz insonation, compared to 1.2 for 80 kHz. Therefore, while low-energy MB-mediated mechanotherapy at a MI below 1.9 could be performed at either 250 or 80 kHz, for NBs, 80 kHz insonation is recommended to maximize low-energy cavitation effects within FDA MI limits. Consequently, 80 kHz US was employed in subsequent NBs-

ablation experiments. Whereas, for sonoporation experiments, lower energy is required and using the 250 kHz center of frequency enables working below the FDA MI upper limit. In vitro, the proximity between MBs/NBs and cells played a crucial role, necessitating molecular targeting of MBs to breast cancer cells due to the propensity of MBs to float rapidly. Therefore, in the tissue-mimicking phantom experiments we compared the effects of low frequency insonation on targeted MBs attached to cells versus free MBs. Results indicated that, due to low-frequency insonation, the impact of cell targeting was not significant, allowing the same parameters to be used for in vitro experiments.

Effects of MB and NBs oscillations on cells viability and molecular uptake were then assessed to evaluate the bioeffect obtained via bubbles oscillations at low frequency US. Note that there is a major difference between MBs and NBs in the context of in vitro assays, where close proximity to the cells is known to play an important role. Since MBs tend to float, free MBs + 80 kHz insonation did not affect cell viability. Thus, cell-targeted MBs were used to achieve close proximity to the cell membrane. NBs do not float immediately, but rather are neutrally buoyant, or move in a Brownian motion within the suspension [83]. Therefore, the NBs used are free NBs without targeting. The choice of conducting experiments in Eppendorf tubes was based on the physical dimensions of the transducer's focal spot. For the center frequency of 250 kHz and 80 kHz, the full width at half maximum for the lateral and axial axes are 7 x 50 mm and 18.9 × 92.7 mm, respectively. Taking advantage of the Eppendorf and focal elongated shapes, conducting the treatment in these tubes enables to treat the entire volume simultaneously without the need to mechanically move the transducer, as required in the case of plates. This approach aligns with in vivo experiments treating the entire tumor simultaneously using the same setup.

In the in vitro studies involving MBs, a concentration of 50 targeted MBs per cell and a treatment duration of 30 seconds were selected. Extending the treatment duration to 180 seconds did not impact cell viability. Hence, to minimize US exposure, a 30-second treatment was preferred. Higher concentrations of targeted MBs were found to increase cellular toxicity without US exposure, leading to the decision not to choose a higher targeted MB

concentration. This phenomenon might be attributed to the phospholipids or the antibody. Studies have previously reported in vitro cytotoxicity at high phospholipid concentrations, and the EPCAM-targeted antibody also exhibited cytotoxicity at elevated concentrations [84,85]. However, it's crucial to note that cells are much more sensitive in vitro, without the supporting biological environment in vivo and that no cell death or off-target toxicity was observed in the targeted MB only control in vivo.

While the MI predicts mechanical bioeffects resulting from cavitation, the CI gauges the level of MB cavitation [86]. The impact of MB insonation on cell viability was assessed at a constant CI of 3.2 (800 kPa for 250 kHz and 250 kPa for 80 kHz). Under these parameters, cell viability after MB-mediated treatment was reduced to 16% for the center frequency of 250 kHz (MI of 1.6), compared to 10% viability for a PNP of 250 kPa (MI of 0.9). This result confirms the advantage of the 80 kHz center frequency, as indicated by tissue-mimicking phantom experiments. In the case of treatment using NBs, despite their smaller size compared to MBs, cell viability dropped to a comparable percentage. Specifically, cell viability was reduced to 17.3 ± 1.7% of live cells for the highest NB concentration tested (12.5×10^7 NBs per µL). No significant changes in cell viability were observed for the control groups, including a sham group, only US, and only NBs (with the same NB concentration of 12.5×10^7 NBs per µL). In the in vitro experiments, NB concentration was provided per milliliter of fluid and not per cell, as the NBs were not directly attached to the cells. A treatment duration of 30 seconds was chosen, as an increase in treatment duration did not enhance cell ablation.

For sonoporation application, we utilized NBs to overcome current limitations associated with the large MBs diameter used in most sonoporation studies. Our approach involves employing low-frequency insonation, unlike the majority of optimization studies in this field that use frequencies exceeding 1 MHz, where strong NB oscillations require PNPs that surpass the FDA safety threshold [51]. The low energy and duty cycles applied ensure that the effect remains purely mechanical and does not induce heat. In this study, we investigated the delivery of four different fluorescent molecules with sizes ranging from 1.2 kDa to 70 kDa, corresponding to substances like chemotherapeutic drugs (1–70 kDa),

siRNA (~14 kDa), and proteins (3–40 kDa) [53]. The ability to deliver large molecules with sonoporation-mediated treatments is closely linked to the US parameters that are used and to NBs concentration, both were optimized in our work. In this study, the initial molecule investigated was 7-AAD (1.2 kDa), a membrane-impermeable dye that undergoes a spectral shift upon binding to DNA. During sonoporation, pores can form in the cell membrane, allowing 7-AAD to enter the cells. NB-mediated sonoporation using low-frequency US results demonstrated a significant increase in the uptake ratio after treatment proving the ability for NBs to induce sonoporation at low energy levels.

NB concentration was calibrated for optimal sonoporation using FITC 4 kDa at a fixed pressure of 300 kPa. The initial concentration of NBs was 1.29×10^7 NBs per µL, and five additional concentrations (2, 4, 8, 12, and 16 times the initial concentration) were tested. The optimal concentration of NBs was found to be 12 times the initial concentration since higher concentration decreased the uptake. The results demonstrated that the combination of US and NBs significantly increased cellular uptake compared to all other control groups, including sham ($p < 0.0001$), free MBs (mixed) + US ($p < 0.0001$), and 12× NB only ($p < 0.0001$). Subsequently, the delivery of larger FITC molecules (4 kDa, 20 kDa, and 70 kDa) was optimized by studying the impact of PNP on sonoporation efficacy. The percentage of fluorescent cells served as a measure to assess delivery efficiency and compare the different sizes of FITC. The highest rate of fluorescent cells resulting from NB sonoporation was observed for the smallest molecules, with approximately 19.9 ± 1.8% of live cells for the FITC 4 kDa molecule. For FITC molecules weighing 20 and 70 kDa, the percentage of fluorescent cells was 14 ± 0.8% and 4.1 ± 1.1% of live cells, respectively. This pattern aligns with the results obtained for targeted MB-mediated sonoporation, where uptake was diminished for larger molecules [52]. To prevent damage to healthy tissue, an upper PNP limit of 800 kPa, resulting in an MI of 1.6, was chosen to ensure compliance with FDA US imaging regulations. The optimal uptake was observed between 300 kPa and 500 kPa, with no significant difference between these pressures for all the tested FITC sizes. Increasing the PNP to 800 kPa led to decreased uptake for all FITC molecules tested. NB-mediated sonoporation achieved a similar efficacy as

targeted MBs for the same pressures and all groups tested ($p > 0.05$), with the only exceptions being the 800 kPa pressures for FITC 4 and 20 kDa, where the targeted MBs groups showed significantly higher uptake ratios ($^*p < 0.05$). However, the maximal uptake was observed at lower PNPs (300–500 kPa). These findings indicate that, despite being smaller in volume by over two orders of magnitude compared to targeted MB, NBs demonstrate similar sonoporation capabilities, whereas NBs were free and did not require any targeting procedures unlike the targeted MBs. All these in vitro results confirm the ability of MBs and NBs to achieve significant bioeffects on cells. However, NBs tumor extravasation ability assessment is another prerequisite step before in vivo evaluation of NB-mediated histotripsy.

To validate the extravasation of NBs into tumor tissue via the EPR effect, cardiac perfusion was conducted 10 minutes after systemic NB injection, followed by harmonic imaging of collected tumors. This aimed to eliminate the NB signal from blood vessels, revealing only the signal of NBs accumulated in the tumor. A contrast enhancement of 10.3 ± 2.5 dB was detected compared to sham tumors without NBs injection. To confirm that this contrast increase resulted from NBs, 80 kHz US treatment was applied to the perfused tumors, leading to NB implosion. A contrast reduction of 8.3 ± 1.0 dB was observed after 80 kHz US application, confirming that the signal in the tumor originated from the presence of NBs in the tumor tissue post-perfusion. No contrast increase was observed in other organs (heart, kidneys, liver, and spleen) after NB systemic injection and cardiac perfusion, indicating that NB extravasation occurs specifically in the tumor due to the EPR effect. Tumor extravasation of NBs was further confirmed by observing the fluorescent NB signal within the tumor tissue following cardiac perfusion.

Tumor ablation experiments using targeted MBs and NBs were conducted on the tumor-bearing mouse model. In vivo, the combination of intratumoral injected targeted MB followed by low-frequency insonation with a MI of 1.6 and 0.9 for 250 kHz and 80 kHz, respectively, reduced tumor viability and created well-defined lesions with large pores in the treated region, as observed in histology. US imaging was employed to visualize tumor-injected targeted MBs before and after low-frequency US treatment, confirming targeted MB

destruction. Quantification of the perforated region on histology revealed a 55% increase in pore size for the 80 kHz frequency compared to 250 kHz ($p < 0.05$). These results suggest that, despite the fact that a center frequency of 80 kHz has a similar CI and a lower MI compared to 250 kHz, higher mechanical damage and tumor cell death are achieved with 80 kHz. Thus, efficient low-energy targeted MB-mediated mechanical tissue fractionation is enhanced at lower frequencies. Next, low-energy tumor ablation mediated by NBs was performed in vivo by applying low-frequency US with a center frequency of 80 kHz only, based on in vitro results. US treatment to breast tumors was performed following NB systemic injection. The method generated significant tumor tissue damage, with visible lesions and tumor fractionation compared to control mice. No damage was observed in internal organs following tumor treatment. The main mechanism for cancer cell fractionation is the implosion of NBs that mechanically ruptures the cells, as observed in histological photomicrographs, where large regions of cellular debris are evident.

4.2 Future work

Our research unveiled a successful approach to achieve low-energy histotripsy and drug delivery of tumors using targeted MBs and NBs in conjunction with low-frequency US. We specifically applied these platforms to breast cancer due to its superficial nature, which facilitates precise US alignment, treatment, and monitoring, making it a practical model for method optimization. To demonstrate versatility, the methods will undergo testing on other tumor types in different locations. In our exploration of NB-mediated ablation, we chose a time point of 10 minutes after NB injection for low-frequency US application, based on a previous study [87]. Although this time point resulted in significant tumor damage, optimization studies will be conducted to refine this parameter. Furthermore, targeted NBs were found to enhance extravasation efficiency, suggesting the potential for applying low-frequency US at later time points after NB injection [88]. This approach could allow for NB clearance from systemic blood circulation while maximizing NB tumor extravasation, potentially improving the method. Moreover, for cancer cells sonoporation based on NB and low frequency US NBs targeting could potentially further enhance the

method and reduce the NBs concentration required for effective drug uptake. Future studies will investigate the impact of the NB-mediated low-energy histotripsy platform on the immune response, exploring its potential combination with adjuvant treatments for metastatic breast cancer. Conventional tumor histotripsy treatments have demonstrated promising immunostimulatory effects, including the release of tumor-associated antigens, increased dendritic and macrophage cell infiltration, heightened CD8+ T-cell responses and suppression of distant metastases [89]. In vivo studies using 4T1 cells with metastatic behavior will assess treatment efficacy through a combination of histotripsy and checkpoint inhibition treatment (aPD-1). The treatment response will be assessed through measurements of tumor growth rate, immunohistochemistry staining to evaluate immune cell infiltration, evaluation of the number of metastases and a survival study. Another project focuses on combining CAR T-cell therapy with NB-mediated low-energy histotripsy to address the challenges faced by CAR-T cell therapy in solid tumors [79]. In contrast to hematological malignancies, where CAR-T cells are easily administered systemically with direct access to the target, applying CAR-T cells to solid tumors encounters significant obstacles. By enhancing CAR-T cell infiltration and modifying the tumor microenvironment through NB-mediated low-energy histotripsy, we aim to improve therapeutic outcomes. In the context of sonoporation applications, our work utilized fluorescent markers as a proxy for efficacy rather than exploring the delivery of therapeutic molecules. Future research should delve into sonoporation of drugs or genetic material. The method's verification was limited to in vitro evaluation, acknowledging that in vivo conditions may introduce additional variables impacting sonoporation effectiveness. Optimization results from the sonoporation study will guide future in vivo research, evaluating the delivery efficiency of NB-mediated low-energy sonoporation in combination with low-frequency US.

4.3 Conclusion

Our findings indicate that lowering the center frequency (80 and 250 kHz) further enhances the oscillations of MBs and NBs, amplifying mechanical treatments such as histotripsy and sonoporation below the FDA MI upper limit

of 1.9 for US imaging applications. In the context of cancer therapy, achieving both high delivery efficacy of therapeutic agents and reducing cell viability are equally crucial. This is because minimizing the tumor burden is essential for the success of cancer treatment [36]. Therefore, in this study, we aimed to achieve multiple outcomes, including enhanced drug delivery via sonoporation and tumor debulking via histotripsy.

Conventional histotripsy utilizes high US energy that can damage any tissue it encounters. For instance breathing movements is a challenge, potentially causing damage to healthy tissues near the focal spot [43]. Moreover, histotripsy procedures are typically performed at a high center frequency, resulting in a reduced focal spot size, requiring mechanical stirring to cover the treated area. In our approach, targeted MBs and NBs are concentrated in the tumor area, and the PNPs used are below the MI of 1.9, reducing the risk of damaging surrounding healthy tissue. Targeted MB concentration into tumors was achieved through invasive intratumoral injection, while NBs were shown to effectively extravasate into tumor tissue following noninvasive systemic injection, enabling noninvasive histotripsy and sonoporation applications when combined with low-frequency US.

The NBs-mediated sonoporation platform demonstrated in this study optimized the relationship between insonation parameters and the size of the delivered molecule, serving as an effective platform for non-invasively delivering large molecules with high spatiotemporal precision. This method could also be applied for gene therapy, where the goal is to introduce new genetic material into cells. Using a large focal spot facilitates patient alignment, shortens treatment duration, and the use of low-frequency insonation is significant to enhance penetration depth for treating deep-seated tumors. Moreover, the methods leverage the advantages of US as a safe, cost-effective, and clinically available modality.

Overall, our research and future work ultimately aim to transform biomedical US for noninvasive cancer therapy. The proposed work opens new avenues for therapeutic applications across various biomedical domains, with the potential to improve patient alignment, shorten treatment duration, and enhanced penetration depth for treating deep-seated tumors.

5. Bibliography

1. Siegel, R.L.; Miller, K.D.; Wagle, N.S.; Jemal, A. Cancer Statistics, 2023. *Ca Cancer J Clin* **2023**, *73*, 17–48.

2. Zhang, J.-F.; Lv, L.; Zhao, S.; Zhou, Q.; Jiang, C.-G. Hyperthermic Intraperitoneal Chemotherapy (HIPEC) Combined with Surgery: A 12-Year Meta-Analysis of This Promising Treatment Strategy for Advanced Gastric Cancer at Different Stages. *Ann. Surg. Oncol.* **2022**, *29*, 3170–3186.

3. Gerritsen, J.; Arends, L.; Klimek, M.; Dirven, C.; Vincent, A. Impact of Intraoperative Stimulation Mapping on High-Grade Glioma Surgery Outcome: A Meta-Analysis. *Acta Neurochir. (Wien).* **2019**, *161*, 99–107, doi:10.1007/s00701-018-3732-4.

4. Tarawneh, A.M.; Pasku, D.; Quraishi, N.A. Surgical Complications and Re-Operation Rates in Spinal Metastases Surgery: A Systematic Review. *Eur. Spine J.* **2021**, *30*, 2791–2799.

5. Pak, H.; Maghsoudi, L.H.; Soltanian, A.; Gholami, F. Surgical Complications in Colorectal Cancer Patients. *Ann. Med. Surg.* **2020**, *55*, 13–18.

6. Xu, Z.; Hall, T.L.; Vlaisavljevich, E.; Lee Jr, F.T. Histotripsy: The First Noninvasive, Non-Ionizing, Non-Thermal Ablation Technique Based on Ultrasound. *Int. J. Hyperth.* **2021**, *38*, 561–575.

7. Fan, Y.; Xu, L.; Liu, S.; Li, J.; Xia, J.; Qin, X.; Li, Y.; Gao, T.; Tang, X. The State-of-the-Art and Perspectives of Laser Ablation for Tumor Treatment. *Cyborg Bionic Syst.* **2023**.

8. Bailey, C.W.; Sydnor, M.K. Current State of Tumor Ablation Therapies. *Dig. Dis. Sci.* **2019**, *64*, 951–958.

9. Kok, H.P.; Cressman, E.N.K.; Ceelen, W.; Brace, C.L.; Ivkov, R.; Grüll, H.; Ter Haar, G.; Wust, P.; Crezee, J. Heating Technology for Malignant Tumors: A Review. *Int. J. Hyperth.* **2020**, *37*, 711–741.

10. Raj, S.; Khurana, S.; Choudhari, R.; Kesari, K.K.; Kamal, M.A.; Garg, N.; Ruokolainen, J.; Das, B.C.; Kumar, D. Specific Targeting Cancer Cells with Nanoparticles and Drug Delivery in Cancer Therapy. In Proceedings of the Seminars in cancer biology; Elsevier, 2021; Vol. 69, pp. 166–177.

11. Saraf, S.; Jain, A.; Tiwari, A.; Verma, A.; Panda, P.K.; Jain, S.K. Advances in Liposomal Drug Delivery to Cancer: An Overview. *J. Drug Deliv. Sci. Technol.*

2020, *56*, 101549.

12. Patnaik, S.; Gorain, B.; Padhi, S.; Choudhury, H.; Gabr, G.A.; Md, S.; Mishra, D.K.; Kesharwani, P. Recent Update of Toxicity Aspects of Nanoparticulate Systems for Drug Delivery. *Eur. J. Pharm. Biopharm.* **2021**, *161*, 100–119.

13. Ghosh, S.; Brown, A.M.; Jenkins, C.; Campbell, K. Viral Vector Systems for Gene Therapy: A Comprehensive Literature Review of Progress and Biosafety Challenges. *Appl. Biosaf.* **2020**, *25*, 7–18.

14. Zhou, Y.; Chen, X.; Cao, J.; Gao, H. Overcoming the Biological Barriers in the Tumor Microenvironment for Improving Drug Delivery and Efficacy. *J. Mater. Chem. B* **2020**, *8*, 6765–6781.

15. Rahmanian, M.; Seyfoori, A.; Ghasemi, M.; Shamsi, M.; Kolahchi, A.R.; Modarres, H.P.; Sanati-Nezhad, A.; Majidzadeh-A, K. In-Vitro Tumor Microenvironment Models Containing Physical and Biological Barriers for Modelling Multidrug Resistance Mechanisms and Multidrug Delivery Strategies. *J. Control. Release* **2021**, *334*, 164–177.

16. Large, D.E.; Abdelmessih, R.G.; Fink, E.A.; Auguste, D.T. Liposome Composition in Drug Delivery Design, Synthesis, Characterization, and Clinical Application. *Adv. Drug Deliv. Rev.* **2021**, *176*, 113851.

17. Kotta, S.; Aldawsari, H.M.; Badr-Eldin, S.M.; Nair, A.B.; Yt, K. Progress in Polymeric Micelles for Drug Delivery Applications. *Pharmaceutics* **2022**, *14*, 1636.

18. Hafeez, M.N.; Celia, C.; Petrikaite, V. Challenges towards Targeted Drug Delivery in Cancer Nanomedicines. *Processes* **2021**, *9*, 1527.

19. Chandrakala, V.; Aruna, V.; Angajala, G. Review on Metal Nanoparticles as Nanocarriers: Current Challenges and Perspectives in Drug Delivery Systems. *Emergent Mater.* **2022**, *5*, 1593–1615.

20. Amin, M.; Lammers, T.; Ten Hagen, T.L.M. Temperature-Sensitive Polymers to Promote Heat-Triggered Drug Release from Liposomes: Towards Bypassing EPR. *Adv. Drug Deliv. Rev.* **2022**, 114503.

21. Seynhaeve, A.L.B.; Amin, M.; Haemmerich, D.; Van Rhoon, G.C.; Ten Hagen, T.L.M. Hyperthermia and Smart Drug Delivery Systems for Solid Tumor Therapy. *Adv. Drug Deliv. Rev.* **2020**, *163*, 125–144.

22. Haider, T.; Pandey, V.; Banjare, N.; Gupta, P.N.; Soni, V. Drug Resistance in

Cancer: Mechanisms and Tackling Strategies. *Pharmacol. Reports* **2020**, *72*, 1125–1151.

23. Zhao, Z.; Ukidve, A.; Kim, J.; Mitragotri, S. Targeting Strategies for Tissue-Specific Drug Delivery. *Cell* **2020**, *181*, 151–167.

24. Kennedy, J.E. High-Intensity Focused Ultrasound in the Treatment of Solid Tumours. *Nat. Rev. cancer* **2005**, *5*, 321–327.

25. Izadifar, Z.; Izadifar, Z.; Chapman, D.; Babyn, P. An Introduction to High Intensity Focused Ultrasound: Systematic Review on Principles, Devices, and Clinical Applications. *J. Clin. Med.* **2020**, *9*, 460.

26. Zhou, Y.-F. High Intensity Focused Ultrasound in Clinical Tumor Ablation. *World J. Clin. Oncol.* **2011**, *2*, 8.

27. Stavarache, M.A.; Chazen, J.L.; Kaplitt, M.G. Innovative Applications of MR-Guided Focused Ultrasound for Neurological Disorders. *World Neurosurg.* **2021**, *145*, 581–589.

28. Todd, N.; McDannold, N.; Borsook, D. Targeted Manipulation of Pain Neural Networks: The Potential of Focused Ultrasound for Treatment of Chronic Pain. *Neurosci. Biobehav. Rev.* **2020**, *115*, 238–250.

29. Meng, Y.; Hynynen, K.; Lipsman, N. Applications of Focused Ultrasound in the Brain: From Thermoablation to Drug Delivery. *Nat. Rev. Neurol.* **2020**, doi:10.1038/s41582-020-00418-z.

30. Sheybani, N.D.; Witter, A.R.; Thim, E.A.; Yagita, H.; Bullock, T.N.J.; Price, R.J. Combination of Thermally Ablative Focused Ultrasound with Gemcitabine Controls Breast Cancer via Adaptive Immunity. *J. Immunother. Cancer* **2020**, *8*.

31. Dell'Italia, J.; Sanguinetti, J.L.; Monti, M.M.; Bystritsky, A.; Reggente, N. Current State of Potential Mechanisms Supporting Low Intensity Focused Ultrasound for Neuromodulation. *Front. Hum. Neurosci.* **2022**, *16*, 872639.

32. Tan, J.-S.; Lin, C.-C.; Chen, G.-S. Vasomodulation of Peripheral Blood Flow by Focused Ultrasound Potentiates Improvement of Diabetic Neuropathy. *BMJ Open Diabetes Res. Care* **2020**, *8*.

33. van den Bijgaart, R.J.E.; Eikelenboom, D.C.; Hoogenboom, M.; Fütterer, J.J.; den Brok, M.H.; Adema, G.J. Thermal and Mechanical High-Intensity Focused Ultrasound: Perspectives on Tumor Ablation, Immune Effects and Combination Strategies. *Cancer Immunol. Immunother.* **2017**, *66*, 247–258.

34. Grutman, T.; Ilovitsh, T. Dense Speed-of-Sound Shift Imaging for Ultrasonic Thermometry. *Phys. Med. Biol.* **2023**, *68*, 215004.

35. Peek, M.C.L.; Ahmed, M.; Napoli, A.; ten Haken, B.; McWilliams, S.; Usiskin, S.I.; Pinder, S.E.; Van Hemelrijck, M.; Douek, M. Systematic Review of High-Intensity Focused Ultrasound Ablation in the Treatment of Breast Cancer. *J. Br. Surg.* **2015**, *102*, 873–882.

36. Fite, B.Z.; Wang, J.; Kare, A.J.; Ilovitsh, A.; Chavez, M.; Ilovitsh, T.; Zhang, N.; Chen, W.; Robinson, E.; Zhang, H.; et al. Immune Modulation Resulting from MR-Guided High Intensity Focused Ultrasound in a Model of Murine Breast Cancer. *Sci. Rep.* **2021**, *11*, 1–15, doi:10.1038/s41598-020-80135-1.

37. Geoghegan, R.; Ter Haar, G.; Nightingale, K.; Marks, L.; Natarajan, S. Methods of Monitoring Thermal Ablation of Soft Tissue Tumors–A Comprehensive Review. *Med. Phys.* **2022**, *49*, 769–791.

38. MacDonell, J.; Patel, N.; Rubino, S.; Ghoshal, G.; Fischer, G.; Burdette, E.C.; Hwang, R.; Pilitsis, J.G. Magnetic Resonance–Guided Interstitial High-Intensity Focused Ultrasound for Brain Tumor Ablation. *Neurosurg. Focus* **2018**, *44*, E11.

39. Mohammadpour, M.; Firoozabadi, B. High Intensity Focused Ultrasound (HIFU) Ablation of Porous Liver: Numerical Analysis of Heat Transfer and Hemodynamics. *Appl. Therm. Eng.* **2020**, *170*, 115014.

40. Krishna, V.; Sammartino, F.; Rezai, A. A Review of the Current Therapies, Challenges, and Future Directions of Transcranial Focused Ultrasound Technology Advances in Diagnosis and Treatment. *JAMA Neurol.* **2018**, *75*, 246–254, doi:10.1001/jamaneurol.2017.3129.

41. Worlikar, T.; Vlaisavljevich, E.; Gerhardson, T.; Greve, J.; Wan, S.; Kuruvilla, S.; Lundt, J.; Ives, K.; Hall, T.; Welling, T.H. Histotripsy for Non-Invasive Ablation of Hepatocellular Carcinoma (HCC) Tumor in a Subcutaneous Xenograft Murine Model. In Proceedings of the 2018 40th Annual International Conference of the IEEE Engineering in Medicine and Biology Society (EMBC); IEEE, 2018; pp. 6064–6067.

42. Khokhlova, V.A.; Fowlkes, J.B.; Roberts, W.W.; Schade, G.R.; Xu, Z.; Khokhlova, T.D.; Hall, T.L.; Maxwell, A.D.; Wang, Y.N.; Cain, C.A. Histotripsy Methods in Mechanical Disintegration of Tissue: Towards Clinical Applications. *Int. J. Hyperth.* **2015**, *31*, 145–162, doi:10.3109/02656736.2015.1007538.

43. Bawiec, C.R.; Khokhlova, T.D.; Sapozhnikov, O.A.; Rosnitskiy, P.B.; Cunitz,

B.W.; Ghanem, M.A.; Hunter, C.; Kreider, W.; Schade, G.R.; Yuldashev, P. V.; et al. A Prototype Therapy System for Boiling Histotripsy in Abdominal Targets Based on a 256-Element Spiral Array. *IEEE Trans. Ultrason. Ferroelectr. Freq. Control* **2020**, *6*, 1, doi:10.1109/TUFFC.2020.3036580.

44. Tran, B.C.; Seo, J.; Hall, T.L.; Fowlkes, J.B.; Cain, C.A. Microbubble-Enhanced Cavitation for Noninvasive Ultrasound Surgery. *IEEE Trans. Ultrason. Ferroelectr. Freq. Control* **2003**, *50*, 1296–1304, doi:10.1109/TUFFC.2003.1244746.

45. Vlaisavljevich, E.; Durmaz, Y.Y.; Maxwell, A.; ElSayed, M.; Xu, Z. Nanodroplet-Mediated Histotripsy for Image-Guided Targeted Ultrasound Cell Ablation. *Theranostics* **2013**, *3*, 851–864, doi:10.7150/thno.6717.

46. Burke, C.W.; Klibanov, A.L.; Sheehan, J.P.; Price, R.J. Inhibition of Glioma Growth by Microbubble Activation in a Subcutaneous Model Using Low Duty Cycle Ultrasound without Significant Heating. *J. Neurosurg.* **2011**, *114*, 1654–1661.

47. Huang, P.; Zhang, Y.; Chen, J.; Shentu, W.; Sun, Y.; Yang, Z.; Liang, T.; Chen, S.; Pu, Z. Enhanced Antitumor Efficacy of Ultrasonic Cavitation with Up-Sized Microbubbles in Pancreatic Cancer. *Oncotarget* **2015**, *6*, 20241.

48. Omata, D.; Unga, J.; Suzuki, R.; Maruyama, K. Lipid-Based Microbubbles and Ultrasound for Therapeutic Application. *Adv. Drug Deliv. Rev.* **2020**, *154*, 236–244.

49. Katz, S.; Gattegno, R.; Peko, L.; Zarik, R.; Hagani, Y.; Ilovitsh, T. Diameter-Dependent Assessment of Microvascular Leakage Following Ultrasound-Mediated Blood-Brain Barrier Opening. *iScience* **2023**, *26*.

50. Kiessling, F.; Fokong, S.; Koczera, P.; Lederle, W.; Lammers, T. Ultrasound Microbubbles for Molecular Diagnosis, Therapy, and Theranostics. *J. Nucl. Med.* **2012**, *53*, 345–348.

51. Rich, J.; Tian, Z.; Huang, T.J. Sonoporation: Past, Present, and Future. *Adv. Mater. Technol.* **2022**, *7*, 2100885.

52. Eck, M.; Aronovich, R.; Ilovitsh, T. Efficacy Optimization of Low Frequency Microbubble-Mediated Sonoporation as a Drug Delivery Platform to Cancer Cells. *Int. J. Pharm. X* **2022**, *4*, 100132.

53. Bismuth, M.; Eck, M.; Ilovitsh, T. Nanobubble-Mediated Cancer Cell

Sonoporation Using Low-Frequency Ultrasound. *Nanoscale* **2023**, *15*, 17899–17909.

54. Delalande, A.; Bastié, C.; Pigeon, L.; Manta, S.; Lebertre, M.; Mignet, N.; Midoux, P.; Pichon, C. Cationic Gas-Filled Microbubbles for Ultrasound-Based Nucleic Acids Delivery. *Biosci. Rep.* **2017**, *37*, BSR20160619, doi:10.1042/bsr20160619.

55. Stewart, K.A.; Navarro, S.M.; Kambala, S.; Tan, G.; Poondla, R.; Lederman, S.; Barbour, K.; Lavy, C. Trends in Ultrasound Use in Low and Middle Income Countries: A Systematic Review. *Int. J. Matern. Child Heal. AIDS* **2020**, *9*, 103.

56. Bez, M.; Foiret, J.; Shapiro, G.; Pelled, G.; Ferrara, K.W.; Gazit, D. Nonviral Ultrasound-Mediated Gene Delivery in Small and Large Animal Models. *Nat. Protoc.* **2019**, *14*, 1015–1026.

57. Ilovitsh, T.; Ilovitsh, A.; Foiret, J.; Caskey, C.F.; Kusunose, J.; Fite, B.Z.; Zhang, H.; Mahakian, L.M.; Tam, S.; Butts-Pauly, K.; et al. Enhanced Microbubble Contrast Agent Oscillation Following 250 KHz Insonation. *Sci. Rep.* **2018**, *8*, 1–15, doi:10.1038/s41598-018-34494-5.

58. Bismuth, M.; Katz, S.; Rosenblatt, H.; Twito, M.; Aronovich, R.; Ilovitsh, T. Acoustically Detonated Microbubbles Coupled with Low Frequency Insonation: Multiparameter Evaluation of Low Energy Mechanical Ablation. *Bioconjug. Chem.* **2021**.

59. Bismuth, M.; Katz, S.; Mano, T.; Aronovich, R.; Hershkovitz, D.; Exner, A.A.; Ilovitsh, T. Low Frequency Nanobubble-Enhanced Ultrasound Mechanotherapy for Noninvasive Cancer Surgery. *Nanoscale* **2022**, *14*, 13614–13627.

60. Glickstein, B.; Aronovich, R.; Feng, Y.; Ilovitsh, T. Development of an Ultrasound Guided Focused Ultrasound System for 3D Volumetric Low Energy Nanodroplet-Mediated Histotripsy. *Sci. Rep.* **2022**, *12*, 20664.

61. Glickstein, B.; Ilovitsh, T. Low Cost and Low Energy 3D Volumetric Histotripsy Using Nanodroplet Vaporization. *J. Acoust. Soc. Am.* **2022**, *152*, A116–A116.

62. Gattegno, R.; Arbel, L.; Riess, N.; Kats, S.; Ilovitsh, T. Enhanced Capillary Delivery with Nanobubble-Mediated Blood-Brain Barrier Opening and Advanced High Resolution Vascular Segmentation. *bioRxiv* **2023**, 2012–2023.

63. Karlinsky, K.T.; Bismuth, M.; Aronovich, R.; Ilovitsh, T. Nonlinear Frequency Mixing Ultrasound Imaging of Nanoscale Contrast Agents. *IEEE Trans. Biomed.*

Eng. **2023**.

64. Ilovitsh, T.; Feng, Y.; Foiret, J.; Kheirolomoom, A.; Zhang, H.; Ingham, E.S.; Ilovitsh, A.; Tumbale, S.K.; Fite, B.Z.; Wu, B.; et al. Low-Frequency Ultrasound-Mediated Cytokine Transfection Enhances T Cell Recruitment at Local and Distant Tumor Sites. *Proc. Natl. Acad. Sci. U. S. A.* **2020**, *117*, 12674–12685, doi:10.1073/pnas.1914906117.

65. Bader, K.B.; Holland, C.K. Gauging the Likelihood of Stable Cavitation from Ultrasound Contrast Agents. *Phys Med Biol* **2013**, *58*, 127–144, doi:10.1088/0031-9155/58/1/127.Gauging.

66. Chowdhury, S.M.; Abou-Elkacem, L.; Lee, T.; Dahl, J.; Lutz, A.M. Ultrasound and Microbubble Mediated Therapeutic Delivery: Underlying Mechanisms and Future Outlook. *J. Control. Release* **2020**, *326*, 75–90.

67. Apfel, R.E.; Holland, C.K. Gauging the Likelihood of Cavitation from Short-Pulse, Low-Duty Cycle Diagnostic Ultrasound. *Ultrasound Med. Biol.* **1991**, *17*, 179–185.

68. Nowicki, A. Safety of Ultrasonic Examinations; Thermal and Mechanical Indices. *Med. Ultrason.* **2020**, *22*, 203–210.

69. Ferrara, K.; Pollard, R.; Borden, M. Ultrasound Microbubble Contrast Agents: Fundamentals and Application to Gene and Drug Delivery. *Annu. Rev. Biomed. Eng.* **2007**, *9*, 415–447, doi:10.1146/annurev.bioeng.8.061505.095852.

70. Bagchi, M.; Moriyama, H.; Shahidi, F. Bio-Nanotechnology: A Revolution in Food, Biomedical and Health Sciences. **2012**.

71. Sawant, R.R.; Torchilin, V.P. Challenges in Development of Targeted Liposomal Therapeutics. *AAPS J.* **2012**, *14*, 303–315.

72. Wu, H.; Abenojar, E.C.; Perera, R.; De Leon, A.C.; An, T.; Exner, A.A. Time-Intensity-Curve Analysis and Tumor Extravasation of Nanobubble Ultrasound Contrast Agents. *Ultrasound Med. Biol.* **2019**, *45*, 2502–2514, doi:10.1016/j.ultrasmedbio.2019.05.025.

73. Helfield, B.; Zou, Y.; Matsuura, N. Acoustically-Stimulated Nanobubbles: Opportunities in Medical Ultrasound Imaging and Therapy. *Front. Phys.* **2021**, *9*, 654374.

74. Qin, S.; Ferrara, K.W. The Natural Frequency of Nonlinear Oscillation of Ultrasound Contrast Agents in Microvessels. *Ultrasound Med. Biol.* **2007**, *33*,

1140–1148, doi:10.1016/j.ultrasmedbio.2006.12.009.

75. Wang, Y.; Li, X.; Zhou, Y.; Huang, P.; Xu, Y. Preparation of Nanobubbles for Ultrasound Imaging and Intracelluar Drug Delivery. *Int. J. Pharm.* **2010**, *384*, 148–153, doi:10.1016/j.ijpharm.2009.09.027.

76. Pulaski, B.A.; Ostrand-Rosenberg, S. Mouse 4T1 Breast Tumor Model. *Curr. Protoc. Immunol.* **2000**, *39*, doi:10.1002/0471142735.im2002s39.

77. Borowsky, A.D.; Namba, R.; Young, L.J.T.; Hunter, K.W.; Hodgson, J.G.; Tepper, C.G.; McGoldrick, E.T.; Muller, W.J.; Cardiff, R.D.; Gregg, J.P. Syngeneic Mouse Mammary Carcinoma Cell Lines: Two Closely Related Cell Lines with Divergent Metastatic Behavior. *Clin. Exp. Metastasis* **2005**, *22*, 47–59, doi:10.1007/s10585-005-2908-5.

78. Costa, E.C.; Moreira, A.F.; de Melo-Diogo, D.; Gaspar, V.M.; Carvalho, M.P.; Correia, I.J. 3D Tumor Spheroids: An Overview on the Tools and Techniques Used for Their Analysis. *Biotechnol. Adv.* **2016**, *34*, 1427–1441.

79. Sterner, R.C.; Sterner, R.M. CAR-T Cell Therapy: Current Limitations and Potential Strategies. *Blood Cancer J.* **2021**, *11*, 69.

80. Hendricks-Wenger, A.; Hutchison, R.; Vlaisavljevich, E.; Allen, I.C. Immunological Effects of Histotripsy for Cancer Therapy. *Front. Oncol.* **2021**, *11*, 681629.

81. Liu, L.; Wang, T.; Lei, B. High-Intensity Focused Ultrasound (HIFU) Ablation versus Surgical Interventions for the Treatment of Symptomatic Uterine Fibroids: A Meta-Analysis. *Eur. Radiol.* **2022**, 1–10.

82. Tsang, S.H.; Ma, K.W.; She, W.H.; Chu, F.; Lau, V.; Lam, S.W.; Cheung, T.T.; Lo, C.M. High-Intensity Focused Ultrasound Ablation of Liver Tumors in Difficult Locations. *Int. J. Hyperth.* **2021**, *38*, 56–64.

83. Meegoda, J.N.; Aluthgun Hewage, S.; Batagoda, J.H. Stability of Nanobubbles. *Environ. Eng. Sci.* **2018**, *35*, 1216–1227.

84. Yin, T.; Wang, P.; Zheng, R.; Zheng, B.; Cheng, D.; Zhang, X.; Shuai, X. Nanobubbles for Enhanced Ultrasound Imaging of Tumors. *Int. J. Nanomedicine* **2012**, *7*, 895.

85. Ruf, P.; Gires, O.; Jäger, M.; Fellinger, K.; Atz, J.; Lindhofer, H. Characterisation of the New EpCAM-Specific Antibody HO-3: Implications for Trifunctional Antibody Immunotherapy of Cancer. *Br. J. Cancer* **2007**, *97*, 315–321.

86. Chu, P.-C.; Chai, W.-Y.; Tsai, C.-H.; Kang, S.-T.; Yeh, C.-K.; Liu, H.-L. Focused Ultrasound-Induced Blood-Brain Barrier Opening: Association with Mechanical Index and Cavitation Index Analyzed by Dynamic Contrast-Enhanced Magnetic-Resonance Imaging. *Sci. Rep.* **2016**, *6*, 1–13.

87. Perera, R.; Hernandez, C.; Cooley, M.; Jung, O.; Jeganathan, S.; Abenojar, E.; Fishbein, G.; Sojahrood, A.J.; Emerson, C.C.; Stewart, P.L. Contrast Enhanced Ultrasound Imaging by Nature-Inspired Ultrastable Echogenic Nanobubbles. *Nanoscale* **2019**, *11*, 15647–15658.

88. Perera, R.; Abenojar, E.; Nittayacharn, P.; Wang, X.; Ramamurthy, G.; Peiris, P.; Bederman, I.; Basilion, J.; Exner, A. Intracellular Vesicle Entrapment of Nanobubble Ultrasound Contrast Agents Targeted to PSMA Promotes Prolonged Enhancement and Stability In Vivo and In Vitro. *bioRxiv* **2021**.

89. Hendricks-Wenger, A.; Sereno, J.; Gannon, J.; Zeher, A.; Brock, R.M.; Beitel-White, N.; Simon, A.; Davalos, R. V; Coutermarsh-Ott, S.; Vlaisavljevich, E. Histotripsy Ablation Alters the Tumor Microenvironment and Promotes Immune System Activation in a Subcutaneous Model of Pancreatic Cancer. *IEEE Trans. Ultrason. Ferroelectr. Freq. Control* **2021**, *68*, 2987–3000.

לתאים הנותרים. התוצאות שהתקבלו היו דומות לאלו עם מיקרובועות שנקשרות לתאים סרטניים, למרות הקוטר הקטן יותר. מכאן שננובועות יכולות לשמש אמצעי יעיל ולא פולשני למתן תרופות.

לסיכום, במחקר אנו מוכיחים שמיקרו- וננובועות יכולים לשמש כגרעיני קוויטציה להרס מכני של גידולים סרטניים בעוצמה נמוכה ולהעברה ממוקדת של תרופות לתאי סרטן, כשהן חשופות לאולטרסאונד בתדר נמוך. השיטות שפותחו מורידות את סף הלחץ הדרוש ביותר מסדר גודל לעומת שיטות ההיסטוטריפסי הרגילות. המחקר שלנו מציג שיטות לא פולשניות לטיפול בסרטן, המבוססות אולטרסאונד בתדר נמוך בשילוב עם חומרי ניגוד מסוג בועות גז ובכך פותח אפיקים חדשים ליישומים רבים בתחומים ביו-רפואיים.

תקציר

אולטרסאונד ממוקד מהווה פלטפורמה טיפולית לא פולשנית בעלת יכולות מגוונות כגון הסרה של גידולים סרטניים או מתן מבוקר וממוקד של תרופות. שיטה נפוצה להסרת גידולים ע"י אולטרסאונד נקראת היסטוטריפסי. בשיטה זו, אשר הינה מכנית ולא מעורב בה חימום, משתמשים באולטרסאונד ממוקד בעוצמה גבוהה במיוחד, באופן מקומי ולא פולשני, כדי לפרק את הרקמה הסרטנית. עם זאת, בהיסטוטריפסי נעשה שימוש בגלי אולטרסאונד ממוקדים בעוצמה גבוהה (לחץ של עשרות מגהפסקל). שימוש בלחצים גבוהים מעלה חשש לבטיחות הטיפול ובייחוד בשל השפעה לא רצויה על אזורים מחוץ לאזור המטרה. במחקר אנו מפתחים שיטות להרס ממוקד של גידולים סרטניים בלחצים נמוכים, תוך שימוש בבועיות גז (מיקרו וננובועות) ואולטרסאונד בתדר נמוך. אנו חוקרים את פעולת הגומלין שקיימת בין בועות ותדר נמוך ככלי להורדת הלחץ הנדרש ופיתוח טכנולוגיות לטיפול בגידולים באופן יעיל בטוח וממוקד. בעת עירור אולטרסאונד, בועיות הגז מבצעות תנודות ובפרמטרים מסוימים אף יכולות להתפוצץ בצורה מבוקרת. תופעה זו יכולה לשחרר אנרגיה בעוצמה גבוהה בסמיכות לבועות, וכך ליצור השפעות ביולוגיות משמעותיות לאזור המטופל, למשל הרס של תאי הגידול הסרטני באזור זה. שיטה זו מספקת מנגנון ייחודי לטיפול באולטרסאונד ממוקד לא פולשני ובעוצמה נמוכה.

המאמר הראשון שלנו מראה שתחת עירור בתדר נמוך (250 ו80 קילו-הרץ), תנודות בעלות אמפליטודה גבוהה של מיקרובועות מתרחשות בלחצים נמוכים משמעותית בהשוואה לתדרי מגה-הרץ הסטנדרטיים. תנודות מוגברות אלו גורמות להרס מקומי של גידולים, וזאת על ידי שימוש באולטרסאונד באנרגיות נמוכות העומד בהנחיות של מנהל המזון והתרופות להדמיית אולטרסאונד. עם זאת, הקוטר הגדול של המיקרובועות (1-4 מיקרומטר) מגביל אותן לשימושים בתוך כלי הדם ולא מחוצה להם, ולכן הן הוזרקו ישירות לגידול בפולשנות מינימלית.

במאמר השני, התגברנו על מגבלה זו באמצעות פיתוח של ננובועות בקוטר של 180 ננומטר. שילוב של אימות ניסיוני ואפיון מקיף של תנודות הננובועות, הובילו לפריצות דרך משמעותיות בטיפול בסרטן השד. הראינו שננובועות מגבירות באופן משמעותי את התנודות שלהן, כאשר הן מעוררות בטווח הקילו-הרץ, וכך סוללות את הדרך לשיטות טיפול חדשניות בסרטן. שילבנו אולטרסאונד בתדר נמוך וננובועות שיכולות לצאת מכלי הדם ולהצטבר בגידול ועל ידי כך יצרנו פלטפורמה טיפולית לא פולשנית לניתוחי סרטן.

במאמר השלישי ניצלנו את ההתנפחות הגדולה של הננובועות בתגובה לעירור בתדר נמוך לצורך פיתוח שיטה לפעירת חורים בממברנות תאי סרטן לשם החדרת תרופות ומולקולות גדולות בצורה לא פולשנית. פלטפורמה זו מהווה אסטרטגיה משולבת לשיפור הטיפול בסרטן, כיוון שמצד אחד היא מקטינה את גודל הגידול ומנגד מצליחה להחדיר תרופות בצורה יעילה

אוניברסיטת תל אביב

הפקולטה להנדסה ע"ש איבי ואלדר פליישמן

בית הספר לתארים מתקדמים ע"ש זנדמן-סליינר

שילוב של אולטרסאונד בתדר נמוך עם בועות גז כפלטפורמה טכנולוגית לטיפול בגידולים

חיבור לשם קבלת התואר" דוקטור לפילוסופיה"

הוגש לסנאט של אוניברסיטת תל אביב

על-ידי

מייק ביסמוט

עבודה זו נעשתה באוניברסיטת תל אביב במחלקה להנדסה ביו-רפואית

בהנחיית ד"ר טלי אילוביץ

שבט תשפ"ד

אוניברסיטת תל אביב

הפקולטה להנדסה ע"ש איבי ואלדר פליישמן

בית הספר לתארים מתקדמים ע"ש זנדמן-סליינר

שילוב של אולטרסאונד בתדר נמוך עם בועות גז כפלטפורמה טכנולוגית לטיפול בגידולים

חיבור לשם קבלת התואר" דוקטור לפילוסופיה"

הוגש לסנאט של אוניברסיטת תל אביב

על-ידי

מייק ביסמוט

עבודה זו נעשתה באוניברסיטת תל אביב במחלקה להנדסה ביו-רפואית

בהנחיית ד"ר טלי אילוביץ

שבט תשפ"ד